Geochemical evidence in the northeast Lau Basin for subduction of the Cook-Austral volcanic chain in the Tonga Trench

Allison Price, Matthew Jackson, Janne Blichert-Toft, Jerzy Blusztajn, Christopher Conatser, Jasper Konter, Anthony A.P. Koppers, Mark Kurz

AGU PUBLICATIONS

Geochemistry, Geophysics, Geosystems

RESEARCH ARTICLE
10.1002/2015GC006237

Key Points:
- Portions of the Rurutu and Rarotonga hotspots likely subducted into the Tonga Trench
- Geochemical signatures in northeast Lau Basin lavas require EM1 and HIMU components
- New high $^{3}He/^{4}He$ lavas are found further to the west in the Lau Basin

Supporting Information:
- Supporting Information S1
- Supporting Information S2
- Data Set S1
- Data Set S2
- Data Set S3
- Data Set S4
- Data Set S5
- Data Set S6
- Data Set S7

Correspondence to:
A. A. Price,
price@umail.ucsb.edu

Citation:
Price, A. A., M. G. Jackson, J. Blichert-Toft, J. Blusztajn, C. S. Conatser, J. G. Konter, A. A.P. Koppers, and M. D. Kurz (2016), Geochemical evidence in the northeast Lau Basin for subduction of the Cook-Austral volcanic chain in the Tonga Trench, *Geochem. Geophys. Geosyst.*, *17*, 1694–1724, doi:10.1002/2015GC006237.

Received 22 DEC 2015
Accepted 18 MAR 2016
Accepted article online 22 MAR 2016
Published online 13 MAY 2016

Geochemical evidence in the northeast Lau Basin for subduction of the Cook-Austral volcanic chain in the Tonga Trench

Allison A. Price[1], Matthew G. Jackson[1], Janne Blichert-Toft[2], Jerzy Blusztajn[3], Christopher S. Conatser[4], Jasper G. Konter[5], Anthony A.P. Koppers[4], and Mark D. Kurz[6]

[1]Department of Earth Science, University of California, Santa Barbara, Santa Barbara, California, USA, [2]Laboratoire de Géologie de Lyon, CNRS UMR 5276, Ecole Normale Supériere de Lyon and Université Claude Bernard Lyon 1, Lyon, France, [3]Department of Geology and Geophysics, Woods Hole Oceanographic Institution, Woods Hole, Massachusetts, USA, [4]College of Earth, Ocean and Atmospheric Sciences, Oregon State University, Corvallis, Oregon, USA, [5]Department of Geology and Geophysics, School of Ocean and Earth Science and Technology, University of Hawaii, Honolulu, Hawaii, USA, [6]Department of Marine Chemistry, Woods Hole Oceanographic Institution, Woods Hole, Massachusetts, USA

Abstract Lau Basin basalts host an array of geochemical signatures that suggest incorporation of enriched mantle source material often associated with intraplate hotspots, but the origin of these signatures remain uncertain. Geochemical signatures associated with mantle material entrained from the nearby Samoan hotspot are present in northwest Lau Basin lavas, and subducted seamounts from the Louisville hotspot track may contribute geochemical signatures to the Tonga Arc. However, lavas in the northeast Lau Basin (NELB) have unique enriched geochemical signatures that cannot be related to these hotspots, but can be attributed to the subduction of seamounts associated with the Cook-Austral volcanic lineament. Here we present geochemical data on a new suite of NELB lavas—ranging in $^{40}Ar/^{39}Ar$ age from 1.3 Ma to 0.365 ka—that have extreme signatures of geochemical enrichment, including lavas with the highest $^{206}Pb/^{204}Pb$ (19.580) and among the lowest $^{143}Nd/^{144}Nd$ (0.512697) encountered in the Lau Basin to date. These signatures are linked to the canonical EM1 (enriched mantle 1) and HIMU (high-μ = $^{238}U/^{204}Pb$) mantle end-members, respectively. Using a plate reconstruction model, we show that older portions of the traces of two of the Cook-Austral hotspots that contributed volcanism to the Cook-Austral volcanic lineament—the Rarotonga and Rurutu hotspots—were potentially subducted in the Tonga Trench beneath the NELB. The geochemical signatures of the Rarotonga, Rurutu, and Samoan hotspots provide a compelling match to the extreme geochemical components observed in the new NELB lavas.

1. Introduction

Spatial and temporal variations in the geochemistry and petrology of back-arc lavas reflect changes in the composition of the mantle wedge that result from the influx of subducted materials and progressive depletion by melt extraction [*Turner and Hawkesworth*, 1998; *Martinez and Taylor*, 2002; *Pearce and Stern*, 2006]. Lavas erupted in back-arc basins globally tend to exhibit geochemically depleted compositions [e.g., *Hart et al.*, 1972; *McCulloch and Gamble*, 1991; *Langmuir et al.*, 2006; *Pearce and Stern*, 2006]. The combined Lau back-arc Basin and Tonga Trench system (Figure 1) is unique, both tectonically and geochemically. The Tonga Trench and the actively spreading Lau back-arc Basin are formed by the westward subduction of the Pacific Plate beneath the Indo-Australian, Niuafo'ou, and Tongan plates [*Zellmer and Taylor*, 2001]. Numerous enriched geochemical components have been detected in the Lau Basin, and these have been variously attributed to the influx of subducted sediments [e.g., *Hergt and Woodhead*, 2007; *Escrig et al.*, 2009, 2012], subducted hotspot tracks such as that of the Louisville seamounts [e.g., *Wendt et al.*, 1997; *Turner and Hawkesworth*, 1997; *Ewart et al.*, 1998; *Falloon et al.*, 2007; *Timm et al*, 2013], and the incorporation of mantle source material from the nearby Samoan plume [e.g., *Poreda and Craig*, 1992; *Turner and Hawkesworth*, 1998; *Price et al.*, 2014].

However, not all geochemical signatures identified in northeast Lau Basin (NELB) lavas can be explained by these processes. Low $^{143}Nd/^{144}Nd$ and radiogenic Pb isotope compositions found in lavas from the NELB require both EMI (enriched mantle 1) and HIMU (high-μ = high $^{238}U/^{204}Pb$) components with values more

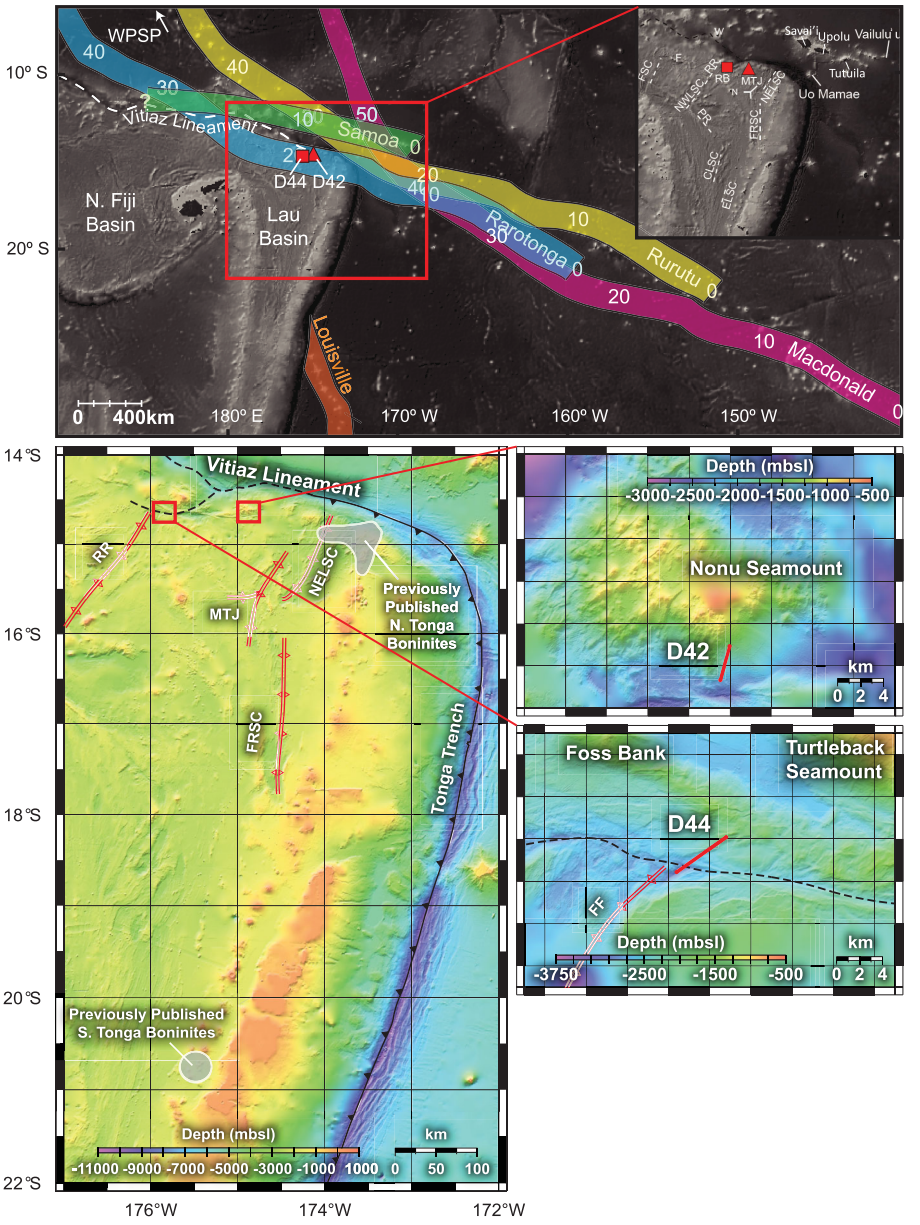

Figure 1. Map of the study region with locations of the dredges (D42 and D44). Hotspot track reconstructions (and ages of the respective hotspot tracks, shown in millions of years) are based on *Wessel and Kroenke* [2008]. Abbreviations: NELB *Northeast Lau Basin*, FSC *Futuna Spreading Center*; F *Futuna Island*; NWLSC *Northwest Lau Spreading Center*; PegR *Peggy Ridge*; RR *Rochambeau Rifts*; RB *Rochambeau Bank*; N *Niua fo'ou*; MTJ *Mangatolu (King's) Triple Junction*; NELSC *Northeast Lau Spreading Center*; FRSC *Fonualei Rift and Spreading Center*; CLSC *Central Lau Spreading Center*; ELSC *Eastern Lau Spreading Center*. (top) Base map was created using GeoMapApp (http://www.geomapapp.org) with topographic and bathymetric data from SRTM_PLUS *Becker et al*. [2009].

extreme than found in Louisville and Samoa [*Falloon et al*., 2007]. *Falloon et al*. [2007] proposed that these anomalous geochemical signatures are due to the subduction of seamounts related to the Cook-Austral volcanic lineament [e.g., *Falloon et al*., 2007; *Regelous et al*., 2008] (discussed in section 4.1.1 below). *Falloon et al*. [2007] suggested that a component from Tubuai Island (from the Macdonald hotspot track), which emerges from the Macdonald hotspot track within the Cook-Austral chain, subducts into the Tonga Trench and imparts its geochemical characteristics to the NELB lavas. Plate reconstructions show that the Macdonald hotspot track does not intersect the Tonga Trench and, therefore, the Macdonald hotspot cannot contribute geochemically to Lau Basin lavas (Figure 1). Rather, two other hotspot trails, the Rurutu and Rarotonga hotspots, which also emerge from the Cook-Austral volcanic lineament (and do intersect the Tonga Trench), may have influenced the geochemistry of the Lau Basin.

Others have referred to the Macdonald hotspot track as the "Tubuai Trend" [*Maury et al*., 2013]. However, this hotspot track has been shown to be anchored by Macdonald seamount, and we refer to it as the Macdonald hotspot track. Similarly, others have referred to the Rurutu hotspot track as the "Atiu trend" [*Maury et al*., 2013]. However, the younger series of volcanism on Rurutu island [e.g., *Chauvel et al*., 1997] anchors the youngest subaerial portion of this hotspot track and we refer to it as the "Rurutu hotspot" track. Here, the Rurutu hotspot includes lavas from Atiu Island, Mauke Island, the young series of volcanics on Rurutu and the younger series of lavas from Arago seamount. The Rarotonga hotspot consists of lavas from Rarotonga Island and the young series of Aitutaki Island. The Macdonald hotspot track does not intersect with the Tonga trench and is not discussed further. It is interesting to note that the older series of volcanism on Rurutu Island has a stronger HIMU flavor and has been linked to the Macdonald hotspot [e.g., *Chauvel et al*., 1997].

We provide geochemical, isotopic, and $^{40}Ar/^{39}Ar$ age data on a suite of lavas dredged from the NELB during the 2013 cruise of the R/V *Roger Revelle* (RR1310). The two dredges (D42 and D44) discussed in this paper are taken 200–300 km west of the Tonga arc (Figure 1 and Table 1) in the NELB. Dredge D42 samples alkalic lavas from a seamount on the northernmost fringe of the Lau Basin that was active between 1.2 and 0.365 Ma. Dredge D44 samples an area located ~20 km southwest of Turtleback Seamount that was active at approximately 1.3 Ma. One subset of the new Lau Basin lavas from dredge D44 reported here hosts the highest $^{206}Pb/^{204}Pb$, and therefore the most extreme HIMU signature, so far encountered in the Lau Basin. A different subset of lavas from dredge D44 has less radiogenic Pb and more geochemically enriched $^{143}Nd/^{144}Nd$ and $^{87}Sr/^{86}Sr$, and are boninitic. These lavas complement previous discoveries of boninites in the Lau Basin and Tonga arc [e.g., *Falloon et al*., 1987; *Sobolev and Danyushevsky*, 1994; *Danyushevsky et al*., 1995; *Falloon and Crawford*, 1991; *Falloon et al*., 2007, 2008; *Cooper et al*., 2010; *Resing et al*., 2011], and mark the westernmost discovery of boninites in the Lau Basin. Additionally, one lava from dredge D44 has relatively high $^{3}He/^{4}He$ (19.3 Ra), which may be a diagnostic geochemical feature of a Samoan influence. While a Samoan component is required for some of the NELB lavas, the geochemical data from the new dredges are best explained if they also host geochemical contributions from two Cook-Austral hotspot components. These two components, from the Rurutu hotspot (HIMU) and the Rarotonga hotspot (EM1), may contribute to the Lau Basin via subduction of older segments of both hotspots. This hypothesis is consistent with plate reconstructions, which show that the reconstructed traces for both the Rurutu and the Rarotonga hotspots intersect the northern Tonga Trench (Figure 1).

2. Methods

2.1. Major Element Analyses

Major element analyses were made on whole rock powders and measured by X-ray fluorescence on a ThermoARL XRF at Washington State University (WSU). The major element data are summarized in Table 1 together with data for an aliquot of the BHVO-2 standard that was run (as an unknown) together with the NELB samples. The precision of SiO_2, Al_2O_3, TiO_2, and P_2O_5 is 0.11–0.33% (1σ) and that of FeO, MgO, CaO, Na_2O, MnO, and K_2O 0.38–0.71% (1σ) of the amount measured [*Johnson and Sinton*, 1990].

2.2. Trace Element Analyses

Trace element concentrations were measured by ICP-MS at WSU on approximately 200 mg of whole rock powders and on two clinopyroxene separates from samples D42-26 and D44-15. The data are reported in Table 1 together with data for a 200 mg aliquot of BHVO-2 that was run (as an unknown) together with the Lau Basin sample unknowns. The precision is 0.77–3.2% (1σ) for all elements except Th (9.5%) and U (9.3%) [*Knaack et al*., 1994; *Hart and Blusztajn*, 2006].

2.3. Hf, Nd, Sr, and Pb Chemical Separation and Mass Spectrometry

Sample leaching, dissolution, column separation, and mass spectrometric analysis of Hf and Pb were carried out at the Ecole Normale Supérieure de Lyon (ENS Lyon). Part of the separation chemistry for Nd and Sr also was carried out at ENS Lyon on the same sample dissolutions as used for Hf and Pb separation, while the final purification steps of Nd and Sr and mass spectrometry analysis were done at Woods Hole Oceanographic Institution (WHOI). The radiogenic isotopic data are reported in Table 2.

Geochemistry, Geophysics, Geosystems

10.1002/2015GC006237

Table 1. Major and Trace Element Analyses of Lavas Examined in this Study

Sample Name			D44-26	D44-15	D44-38	D44-46	D44-91	D42-60	D42-25	D42-05	D42-30	D42-20	D42-26	BHVO-2[c]
Material analyzed[a]			Whole rock powder	Basaltic clinopyroxene	Whole rock powder	Whole rock powder	Whole rock powder	Whole rock powder	Whole rock powder	Whole rock powder	Whole rock powder	Whole rock powder	Olivine websterite xenolith clinopyroxene	Standard USGS powder
Dredge on bottom (Lat)			−14.659°	−14.659°	−14.659°	−14.659°	−14.659°	−14.678°	−14.678°	−14.678°	−14.678°	−14.678°	−14.678°	–
Dredge on bottom (Lon)			−175.860°	−175.860°	−175.860°	−175.860°	−175.860°	−174.891°	−174.891°	−174.891°	−174.891°	−174.891°	−174.891°	–
Dredge off bottom (Lat)			−14.632°	−14.632°	−14.632°	−14.632°	−14.632°	−14.651°	−14.651°	−14.651°	−14.651°	−14.651°	−14.651°	–
Dredge off bottom (Lon)			−175.820°	−175.820°	−175.820°	−175.820°	−175.820°	−174.884°	−174.884°	−174.884°	−174.884°	−174.884°	−174.884°	–
Dredge Length			5.30 km	5.30 km	5.30 km	5.30 km	5.30 km	3.09 km	3.09 km	3.09 km	3.09 km	3.09 km	3.09 km	–
Dredge Depth (average)			2790 m	2790 m	2790 m	2790 m	2790 m	2210 m	2210 m	2210 m	2210 m	2210 m	2210 m	–
SiO_2	**(wt.%)**	**XRF**	54.35	-	58.89	57.33	49.21	48.08	45.62	44.97	48.34	47.89	-	49.78
TiO_2	**(wt.%)**	**XRF**	1.14	-	0.38	0.36	1.65	1.74	1.88	1.95	1.75	1.86	-	2.75
Al_2O_3	**(wt.%)**	**XRF**	18.42	-	13.25	12.43	15.18	15.78	12.80	12.50	15.94	15.01	-	13.53
FeO_{tot}	**(wt.%)**	**XRF**	6.59	-	8.24	8.42	10.74	9.88	9.70	9.96	9.74	9.41	-	11.24
MnO	**(wt.%)**	**XRF**	0.12	-	0.15	0.16	0.18	0.17	0.17	0.18	0.18	0.16	-	0.17
MgO	**(wt.%)**	**XRF**	3.40	-	6.19	8.22	9.05	7.69	11.22	11.42	7.57	9.07	-	7.22
CaO	**(wt.%)**	**XRF**	9.08	-	8.92	9.35	10.50	9.70	11.33	11.42	9.83	10.52	-	11.35
Na_2O	**(wt.%)**	**XRF**	3.53	-	1.94	1.64	2.60	3.26	2.87	2.64	3.28	3.05	-	2.23
K_2O	**(wt.%)**	**XRF**	0.90	-	0.99	0.78	0.39	1.95	2.07	2.00	1.84	1.53	-	0.51
P_2O_5	**(wt.%)**	**XRF**	0.41	-	0.13	0.11	0.15	0.45	0.64	0.70	0.44	0.51	-	0.26
Sum	**(wt.%)**	**XRF**	97.94	-	99.09	98.80	99.63	98.70	98.30	97.74	98.92	99.01	-	99.05
LOI %	**(wt.%)**	**XRF**	0.97	-	0.28	0.38	0.00	0.79	0.81	0.76	0.07	0.00	-	0.00
Mg#[b]			0.38	-	0.47	0.53	0.50	0.48	0.58	0.57	0.48	0.53	-	0.43
Ni	**(ppm)**	**XRF**	35	-	44	72	200	93	195	200	86	155	-	114
Cr	**(ppm)**	**XRF**	52	-	223	373	380	336	633	658	335	428	-	276
Sc	**(ppm)**	**XRF**	26	-	38	39	37	24	32	33	25	30	-	31
V	**(ppm)**	**XRF**	259	-	264	254	280	196	245	246	201	231	-	314
Ba	**(ppm)**	**XRF**	598	-	307	241	56	770	1011	973	790	744	-	134
Rb	**(ppm)**	**XRF**	17	-	19	14	6	54	56	53	52	42	-	9
Sr	**(ppm)**	**XRF**	606	-	399	303	141	678	716	725	681	677	-	387
Zr	**(ppm)**	**XRF**	113	-	46	36	105	159	148	148	158	147	-	164
Y	**(ppm)**	**XRF**	22	-	10	11	35	23	23	23	24	24	-	27
Nb	**(ppm)**	**XRF**	41	-	8	6	6	40	43	42	41	39	-	18
Ga	**(ppm)**	**XRF**	18	-	13	12	17	19	16	16	19	17	-	20
Cu	**(ppm)**	**XRF**	88	-	110	69	86	41	61	74	43	43	-	128
Zn	**(ppm)**	**XRF**	76	-	69	67	89	106	85	86	104	85	-	99
Cs	**(ppm)**	**ICP**	0.26	0.01	0.4	0.28	0.07	0.99	1.02	0.94	0.59	0.43	0.01	0.1
Rb	**(ppm)**	**ICP**	16.30	0.60	18.60	14.20	6.70	52.70	55.60	53.60	51.50	40.60	1.80	9.20
Ba	**(ppm)**	**ICP**	598.0	15.0	312.0	237.0	51.0	766.0	1004.0	974.0	775.0	743.0	47.0	129.0
Th	**(ppm)**	**ICP**	7.07	0.16	3.13	2.22	0.52	5.36	5.90	5.92	5.44	6.03	1.26	1.23
U	**(ppm)**	**ICP**	1.94	0.04	0.85	0.60	0.15	1.37	1.65	1.63	1.17	1.11	0.32	0.41
Nb	**(ppm)**	**ICP**	40.25	1.19	5.98	3.92	5.00	39.36	41.61	42.11	39.29	37.66	10.49	16.95
Ta	**(ppm)**	**ICP**	2.09	0.08	0.33	0.23	0.38	2.46	2.44	2.47	2.46	2.22	0.68	1.17
La	**(ppm)**	**ICP**	46.76	2.50	17.16	11.40	5.86	40.13	49.64	50.41	40.06	45.60	10.46	15.44
Ce	**(ppm)**	**ICP**	82.5	6.6	28.6	19.9	15.2	77.0	97.6	100.3	77.7	84.1	21.1	37.5
Pb	**(ppm)**	**ICP**	8.31	0.16	4.98	3.69	0.72	5.36	5.73	5.81	5.34	4.67	0.40	1.64
Pr	**(ppm)**	**ICP**	8.85	0.99	3.16	2.33	2.33	9.03	11.47	11.87	9.12	9.57	2.43	5.33
Nd	**(ppm)**	**ICP**	32.0	5.0	11.8	8.8	11.7	34.5	44.2	45.5	34.9	36.3	9.9	24.5
Sr	**(ppm)**	**ICP**	606.0	55.0	405.0	307.0	144.0	684.0	723.0	743.0	686.0	681.0	189.0	393.0
Zr	**(ppm)**	**ICP**	117.0	10.0	47.0	37.0	108.0	164.0	154.0	156.0	163.0	152.0	43.0	169.0
Hf	**(ppm)**	**ICP**	2.72	0.36	1.19	0.98	2.82	4.11	3.91	3.91	4.19	3.85	1.12	4.40
Sm	**(ppm)**	**ICP**	5.75	1.49	2.30	1.92	3.98	7.07	8.22	8.35	7.11	7.13	2.37	6.38
Eu	**(ppm)**	**ICP**	1.73	0.49	0.69	0.58	1.43	2.19	2.49	2.57	2.27	2.27	0.78	2.18
Gd	**(ppm)**	**ICP**	4.82	1.54	1.99	1.74	5.12	6.23	6.57	6.77	6.20	6.40	2.31	6.45

Geochemistry, Geophysics, Geosystems
10.1002/2015GC006237

Table 1. (continued)

Sample Name			D44-26	D44-15	D44-38	D44-46	D44-91	D42-60	D42-25	D42-05	D42-30	D42-20	D42-26	BHVO-2[c]
Material analyzed[a]			Whole rock powder	Basaltic clinopyroxene	Whole rock powder	Whole rock powder	Whole rock powder	Whole rock powder	Whole rock powder	Whole rock powder	Whole rock powder	Whole rock powder	Olivine websterite xenolith clinopyroxene	Standard USGS powder
Tb	**(ppm)**	**ICP**	0.72	0.24	0.30	0.27	0.96	0.91	0.91	0.94	0.92	0.95	0.36	1.00
Dy	**(ppm)**	**ICP**	4.21	1.42	1.74	1.66	6.29	5.05	4.93	4.97	5.05	5.24	2.10	5.70
Ho	**(ppm)**	**ICP**	0.83	0.28	0.36	0.35	1.34	0.93	0.88	0.91	0.93	0.96	0.40	1.07
Y	**(ppm)**	**ICP**	21.1	7.9	9.3	8.8	33.6	23.2	21.6	22.3	23.2	24.7	11.7	26.0
Er	**(ppm)**	**ICP**	2.21	0.70	1.00	0.96	3.75	2.28	2.13	2.17	2.34	2.47	1.02	2.59
Tm	**(ppm)**	**ICP**	0.31	0.09	0.15	0.15	0.55	0.31	0.29	0.29	0.31	0.34	0.14	0.35
Yb	**(ppm)**	**ICP**	1.95	0.54	0.96	0.98	3.36	1.83	1.66	1.67	1.86	1.97	0.85	1.95
Lu	**(ppm)**	**ICP**	0.31	0.08	0.16	0.17	0.54	0.29	0.25	0.25	0.30	0.29	0.13	0.28
Sc	**(ppm)**	**ICP**	26.20	94.70	38.90	40.10	38.50	24.30	34.20	33.70	25.30	29.20	70.10	31.50

With the exception of the BHVO-2 USGS reference material, all samples have the prefix RR1310.

[a]Major elements and Ni, Cr, Sc, V, Ba, Rb, Sr, Zr, Y, Nb, Ga, Cu, and Zn were measured by XRF. A subset of these trace elements, and a suite of additional trace elements, were measured by ICP-MS. Clinopyroxenes were separated from a basalt (sample D44-26) and a websterite xenolith (sample D42-26) for trace element and Sr, Nd, and Pb isotopic analyses (see Table 2).

[b]Mg# = molar ratio of MgO/(MgO + 0.85 * FeO)

[c]Sample was provided to Washington State Univeristy Geoanalytical Lab as an unknown.

Geochemistry, Geophysics, Geosystems

10.1002/2015GC006237

Table 2. Sr, Nd, Hf and Pb Isotopic Analyses on Northeast Lau Basin Lavas[a]

Sample Name	Lithology	Designation in Text	Phase Analyzed for Hf-Pb-Sr-Nd	$^{86}Sr/^{87}Sr$[b]	Error (2σ)[c]	$^{143}Nd/^{144}Nd$[b]	Error (2σ)[c]	εNd[d]	$^{176}Hf/^{177}Hf$[b]	Error (2σ)[c]	εHf[d]	$^{206}Pb/^{204}Pb$[b]	Error (2σ)[c]	$^{207}Pb/^{204}Pb$[b]	Error (2σ)[c]	$^{208}Pb/^{204}Pb$[b]	Error (2σ)[c]
D44-26	Magnesian andesite	D44-HIMU	WR[e]	0.704087	0.000006	0.512784	0.000010	2.8	0.282991	0.000005	7.7	19.5800	0.0006	15.6636	0.0004	39.4132	0.0012
D44-15	CPX	D44-HIMU	CPX[e]	0.704080	0.000007	0.512778	0.000008	2.7	-	-	-	19.4636	0.0053	15.6549	0.0051	39.3350	0.0122
D44-38	Boninite	D44-EM	WR	0.704564	0.000005	0.512798	0.000009	3.1	0.283071	0.000004	10.6	19.1903	0.0006	15.6424	0.0006	39.0950	0.0014
D44-46	Boninite	D44-EM	WR	0.704488	0.000011	0.512793	0.000011	3.0	0.283073	0.000004	10.6	19.0785	0.0008	15.6250	0.0007	38.9905	0.0019
D44-91	Tholeiite basalt	D44-Depleted	WR	0.704008	0.000008	0.512889	0.000006	4.9	0.283109	0.000004	11.9	18.6369	0.0008	15.5701	0.0007	38.6386	0.0017
D42-60	Alkali basalt	D42	WR	0.704058	0.000004	0.512750	0.000007	2.2	0.282940	0.000004	5.9	19.1277	0.0007	15.6389	0.0006	39.1334	0.0016
D42-25	Alkali basalt	D42	WR	0.704233	0.000012	0.512697	0.000005	1.2	0.282909	0.000005	4.8	19.1337	0.0006	15.6400	0.0005	39.1608	0.0012
D42-05	Alkali basalt	D42	WR	0.704221	0.000009	0.512711	0.000006	1.4	0.282912	0.000005	4.9	19.1619	0.0007	15.6425	0.0005	39.1769	0.0014
D42-30	Alkali basalt	D42	WR	0.704065	0.000006	0.512790	0.000008	3.0	0.282952	0.000004	6.4	19.1272	0.0005	15.6395	0.0004	39.1378	0.0012
D42-20	Alkali basalt	D42	WR	0.704148	0.000006	0.512767	0.000015	2.5	0.282968	0.000004	6.9	19.1529	0.0009	15.6405	0.0006	39.1683	0.0018
D42-26	Xenolith[f]	D42	CPX	0.703871	0.000005	0.512774	0.000015	2.7	-	-	-	19.1029	0.0029	15.6406	0.0067	39.0981	0.0067
BCR-2[g]	Basalt	-	WR	-	-	-	-	-	0.282886	0.000003	4.0	18.7558	0.0009	15.6251	0.0008	38.7414	0.0022
AGV-2[g]	Andesite	-	WR	-	-	-	-	-	0.282988	0.000006	7.6	18.866	0.0009	15.6174	0.0009	38.5299	0.0032

[a]With the exception of the BCR-2 and AGV-2 USGS rock standards, all samples have the prefix RR1310.

[b]Nd isotopic compositions are corrected to the La Jolla value of 0.511847. Sr isotopic compositions are corrected to the NBS 987 value of 0.710240. Pb isotopic compositions are corrected to the NIST 981 values of *Eisele et al.* [2003] ($^{206}Pb/^{204}Pb = 16.9409$, $^{207}Pb/^{204}Pb = 15.4976$, and $^{208}Pb/^{204}Pb = 36.7262$). The unweighted mean $^{176}Hf/^{177}Hf$ of the JMC-475 Hf standard run alternately with the samples gave 0.282170 ± 0.000010, which is identical within error to the preferred value of 0.282163 ± 0.000009 [*Blichert-Toft et al.*, 1997], hence no corrections were applied to the $^{176}Hf/^{177}Hf$ data.

[c]Error is 2σ standard error of the mean, and is absolute (not relative). Errors represent internal (in-run) precision.

[d]The Nd and Hf epsilon notations were calculated using the CHUR values of $^{143}Nd/^{144}Nd = 0.512638$ [*Wasserburg et al.*, 1981] and $^{176}Hf/^{177}Hf = 0.282772$ [*Blichert-Toft and Albarède*, 1997].

[e]WR = whole rock; CPX = clinopyroxene.

[f]Olivine websterite xenolith found in dredge-D42 consists of ~60% orthopyroxene, 26% olivine, 10% clinopyroxene, and 4% spinel.

[g]BCR-2 and AGV-2 were processed together with the sample unknowns.

Hafnium, Nd, Sr, and Pb isotopic data were obtained from 200 to 450 mg of whole rock lava chips (or clinopyroxene separated from lavas) for the 11 samples constituting this study. With one exception (sample D44-15), all samples were exceptionally fresh and showed little evidence of submarine alteration. Sample D44-15, a submarine lava, is altered (see sample descriptions in supporting information), and hence fresh clinopyroxene was separated for radiogenic isotopic analyses. Clinopyroxene also was separated for radiogenic isotopic analyses from sample D42-26 (an olivine websterite xenolith hosted in a basaltic lava).

All samples were acid leached prior to digestion using the following protocol: the samples were first leached in 1 mL of 30% Suprapur H_2O_2 for 15 min at 130°C, followed by 15 min of sonication, and an additional 10 min at 130°C. The H_2O_2 was pipetted off and the samples rinsed with milliQ H_2O. The samples were then leached in 2 mL of 6*M* HCl for 1 h at 130° C, followed by 10 minutes of sonication and another 10 minutes of heating at 130°C; the HCl was pipetted off and the samples rinsed twice in milliQ H_2O. The samples were finally leached in 2 mL of 4*M* HNO_3 for 1 h at 130°C, followed by 15 min sonication and an additional 10 min at 130°C; the HNO_3 was pipetted off and the samples rinsed twice in milliQ H_2O.

All samples were dissolved in a 3:1 mixture of concentrated double-distilled HF and HNO_3. After digestion and evaporation to dryness, Hf was separated from the rest of the sample by leaching for 48 h with concentrated double-distilled HF and then taking the HF supernatant containing the Hf through two successive anion and cation-exchange columns following the methods outlined in *Blichert-Toft et al*. [1997]. Accidental application of this method on the two clinopyroxene separates of this study led to the regrettable result, as already known from *Blichert-Toft* [2001], that Hf was not properly separated for these two samples and hence could not be analyzed for its isotopic composition with sufficient accuracy and precision. The CaMg-fluoride precipitate resulting from the HF leaching step (which contains most of the Pb, Sr, and Nd) [*Blichert-Toft et al*., 1997] was loaded onto microcolumns filled with 0.5 mL AG1-X8 resin (100–200 mesh). Strontium and Nd were recovered from the clean wash of these columns using 1*M* HBr, while Pb was eluted with 6*M* HCl. At WHOI, the Sr-Nd fraction was split in two, and one fraction was taken through Eichrom Sr-spec resin loaded on 300 μL columns for Sr separation and the other fraction was taken through Eichrom Ln-spec columns for Nd separation. The total procedural blanks for Hf, Pb, Sr, and Nd were $<$ 20 pg, $<$ 25 pg, $<$ 50 pg, and $<$ 35 pg, respectively, which are all negligible relative to the amounts of Hf, Pb, Sr, and Nd analyzed.

Hafnium and Pb isotopic compositions were determined by multicollector inductively coupled plasma mass spectrometry (MC-ICP-MS) on the Nu Plasma 500 HR at ENS Lyon, while Sr and Nd isotopic compositions were measured on the Neptune MC-ICP-MS at WHOI as follows:

2.3.1. Hafnium

Hafnium isotopic measurements followed the protocol described by *Blichert-Toft et al*. [1997]. The JMC-475 Hf standard was analyzed every second sample and the unweighted mean $^{176}Hf/^{177}Hf$ obtained during a daylong analytical session was 0.282170 $\pm$ 0.000010 (i.e., external 2σ precision of 30 ppm). Since this value is identical within error to the accepted value of 0.282163 $\pm$ 0.000009 [*Blichert-Toft et al*., 1997] for JMC-475, no corrections were applied to the Lau Basin data. Although insignificant for all analyzed samples, the Hf isotopic ratios were corrected online for isobaric interferences of W and Ta on mass 180 and of Lu and Yb on mass 176 by monitoring the interference-free isotopes ^{183}W, ^{181}Ta, ^{175}Lu, and ^{173}Yb, respectively. Sample and standard data were corrected for instrumental mass fractionation relative to $^{179}Hf/^{177}Hf$ of 0.7325 using an exponential law.

2.3.2. Lead

Lead isotopic ratios were measured using Tl doping and sample-standard bracketing and the values for NIST 981 of *Eisele et al*. [2003] (16.9409 for $^{206}Pb/^{204}Pb$, 15.4976 for $^{207}Pb/^{204}Pb$, and 36.7262 for $^{208}Pb/^{204}Pb$). The external precision of the reported Pb isotope ratios is 100–200 ppm (2σ) (or 0.01–0.02%).

2.3.3. Strontium

Intensities were measured on masses 82 through 88 and corrections for isobaric interferences on masses 87 (Rb), 84 (Kr), and 86 (Kr) were made offline following the procedures outlined in *Jackson and Hart* [2006]. Strontium isotopic ratios were corrected for instrumental mass bias relative to $^{86}Sr/^{88}Sr$ of 0.1194 using an exponential law. Measured sample $^{87}Sr/^{86}Sr$ ratios were normalized to $^{87}Sr/^{86}Sr$ of 0.710240 [*Jackson and Hart*, 2006] for SRM 987. Based on the repeated measurements of the SRM 987 standard analyzed during each analytical session, external precision of the $^{87}Sr/^{86}Sr$ measurements are better than 25 ppm.

2.3.4. Neodymium

Neodymium isotopic compositions were corrected for instrumental mass fractionation relative to $^{146}Nd/^{144}Nd$ of 0.7219 using an exponential law. The JNdi-1 Nd and La Jolla standards were run during

Table 3. He Isotopic Analyses on Northeast Lau Basin Lavas[a]

Sample Name	Designation in Text	Phase Analyzed for He	3He/4He (R/Ra)	Error (2σ)[b]	[4He] 10−9 cc STP/g
D44-26	D44-HIMU	CPX[c]	7.77	0.3	6.7
D44-15	D44-HIMU	Olivine	7.69	0.39	4.6
D44-38	D44-EM	Olivine	7.98	0.36	3.1
D44-46	D44-EM	Olivine	7.9	0.57	1
D44-91	D44-Depleted	Glass	19.33	0.56	996
D42-25	D42	Glass	3.79	0.14	15
D42-26	D42 xenolith	Olivine	7.89	0.23	1260
D42-15	D42	Glass	2.84	0.1	24

[a]All samples have the prefix RR1310.
[b]Error is 2σ standard error of the mean, and is absolute (not relative). Errors represent internal (in-run) precision.
[c]CPX = clinopyroxene.

each analytical session. The $^{143}Nd/^{144}Nd$ values for JNdi-1 were adapted to the La Jolla $^{143}Nd/^{144}Nd$ value using a ratio of 1.000503 [*Tanaka et al*., 2000]. The La Jolla and La Jolla-renormalized JNdi-1 $^{143}Nd/^{144}Nd$ measurements were averaged to give a final La Jolla average for the analytical session, which in turn, was used to normalize the sample $^{143}Nd/^{144}Nd$ relative to a preferred La Jolla $^{143}Nd/^{144}Nd$ of 0.511847 [*White and Patchett*, 1984]. Based on the repeated measurements of the JNdi-1 standard analyzed during each analytical session, external precision of the $^{143}Nd/^{144}Nd$ measurements are better than 20 ppm.

USGS reference materials, BCR-2 and AGV-2, were dissolved, processed, and analyzed with unknowns (although rock standards were not leached). The BCR-2 reference material measured in this study gave $^{176}Hf/^{177}Hf$ of 0.282886 ± 4, which is identical within the quoted uncertainties to the value of 0.282884 ± 7 (2σ) reported by *Le Fèvre and Pin* [2001]. Results for Pb isotopic measurements of the BCR-2 and AGV-2 rock standards likewise compare well with those of *Weis et al*. [2006] (see Table 2). Note for purposes of comparison that we present Pb isotopic data normalized to NIST 981 values from *Eisele et al*. [2003], while *Weis et al*. [2006] normalize to values from *Abouchami et al*. [2000].

2.4. He Isotopic Analyses

Helium isotopes were measured on fresh glass, olivine, and clinopyroxene separates at WHOI using an automated dual-collection, statically operated He isotope mass spectrometer. All measurements were made by crushing in vacuo following the protocol of *Kurz et al*. [2004]. Helium concentrations (^4He) released by crushing ranged from 1.0×10^{-9} to 1.26×10^{-6} cc STP/g, and internal precision of the $^3He/^4He$ measurements ranged from ±0.10 to ±0.57 Ra (2σ). $^3He/^4He$ ratios are reported relative to atmospheric (R/Ra) using an atmospheric $^3He/^4He$ ratio of 1.384×10^{-6}. The $^3He/^4He$ data are listed in Table 3.

2.5. $^{40}Ar/^{39}Ar$ Geochronology Analyses

$^{40}Ar/^{39}Ar$ ages were obtained by incremental heating methods on groundmass and plagioclase separates at Oregon State University. Samples were prepared by sawing, crushing, magnetic separation, acid leaching, and handpicking according to the methods described in *Koppers et al*. [2011]. Seven samples were irradiated for 6 h (14-OSU-04) in the TRIGA nuclear reactor at Oregon State University, along with the Fish Canyon Tuff sanidine age standard (28.201 ± 0.023 Ma from *Kuiper et al*. [2008]) to measure the required J-values for the age calibration (~0.15% 1σ uncertainties). The $^{40}Ar/^{39}Ar$ data are listed in Table 4 and age spectra are shown in Figure 2; full data sets are provided in the supporting information.

The $^{40}Ar/^{39}Ar$ incremental heating age determinations were performed on a multicollector ARGUS-VI mass spectrometer with five Faraday collectors (all fitted with 10^{12} Ohm resistors) and one ion-counting CuBe electron multiplier. Collector calibrations (for mass 36, intercalibrated by alternating measurements on the multiplier and the adjacent Faraday cup) were carried out by measuring air shots (daily) for typical intensity ranges, and the calibrations were applied to all unknown samples, flux monitors, and measured blanks. Irradiated samples were loaded into Cu-planchettes in an ultrahigh vacuum sample chamber and incrementally heated by scanning a defocused 25 W CO_2 laser beam in preset patterns across the sample, in order to release the argon evenly. After heating, reactive gases were cleaned up for ~6 min using an SAES Zr-Al

Geochemistry, Geophysics, Geosystems
10.1002/2015GC006237

Table 4. Summary of $^{40}Ar/^{39}Ar$ Age Analysis[a]

Sample Information				Plateau						Inverse Isochron			Inverse Isochron	
Experiment Number	Sample ID	Location	Material	Age ± 2σ	^{39}Ar (%)	K/Ca	MSWD	n	N	Age ± 2σ	$^{40}Ar/^{36}Ar$ Intercept	MSWD	Age ± 2σ	K/Ca
14D29547	D42-02	Lau Basin	Groundmass	364.8 ± 3.7 ka	100	0.087	0.93	33	33	364.0 ± 5.8 ka	296.18	0.96	365.8 ± 4.3 ka	0.293
14D32259	D42-67	Lau Basin	Groundmass	599.9 ± 5.6 ka	65.56	1.155	1.95	19	33	585.8 ± 7.8 ka	307.7	0.91	590.9 ± 4.9 ka	0.494
14D32303	D42-68	Lau Basin	Groundmass	644.5 ± 5.9 ka	51.22	1.187	1.17	16	33	649.2 ± 7.8 ka	292.65	1.04	654.4 ± 8.1 ka	0.435
14D32211	D42-60	Lau Basin	Groundmass	1223.2 ± 19.0 ka	87.65	0.074	2.31	17	36	1224.4 ± 39.0 ka	295.02	2.44	1297.3 ± 29.6 ka	0.091
14D29619	D44-08	Lau Basin	Plagioclase	1249.1 ± 50.9 ka	82.61	0.015	1.11	14	21	1358.9 ± 162.6 ka	286.73	1.05	1316.7 ± 48.2 ka	0.014
15D04155	D44-12	Lau Basin	Groundmass						33				1535.6 ± 29.9 ka	0.116
14D33125	D44-26	Lau Basin	Plagioclase	1278.8 ± 115.3 ka	100	0.005	0.5	21	21	1363.8 ± 268.6 ka	292.71	0.51	1270.9 ± 117.4 ka	0.005

[a]Summary of $^{40}Ar/^{39}Ar$ age analysis on seven groundmass and/or plagioclases from dredges RR1310-D42 and D44. All samples have the prefix RR1310. K/Ca values are calculated as weighted means for the age spectra or as total fusion K/Ca values by combining the gas analyses. Both the number of steps (n) included in the age plateau and isochron calculations and the total number of incremental heating steps (N) have been listed. MSWD values for the age plateaus and inverse isochrons are calculated using n-1 and n-2 degrees of freedom, respectively. All samples were monitored against FCT-NM sanidine (28.201 ± 0.023 Ma, 1σ) as calibrated by *Kuiper et al.* [2008]. The $^{40}Ar/^{39}Ar$ ages are weighted age estimates with errors reported at the 95% confidence level, including 0.15% standard deviations in the J-value.

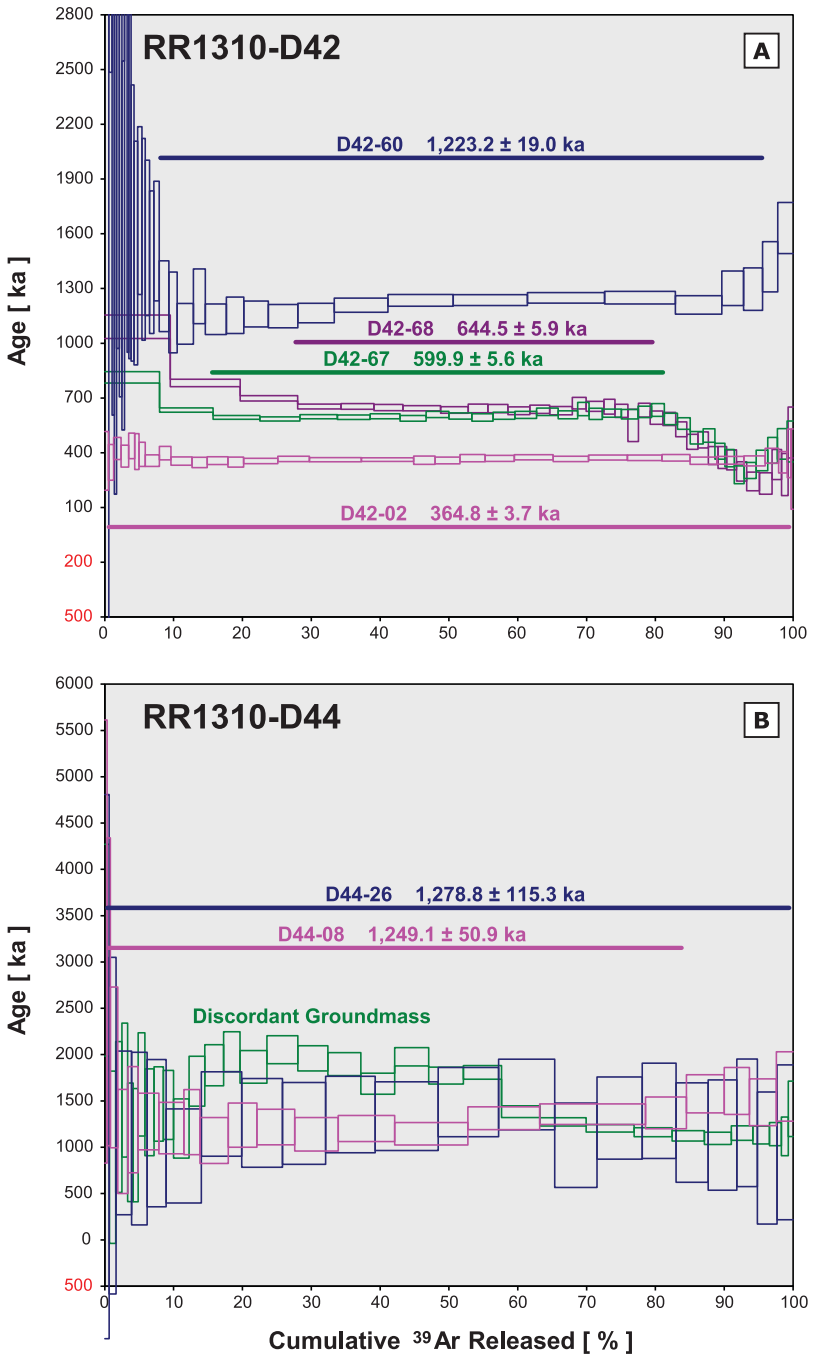

Figure 2. High-resolution incremental heating $^{40}Ar/^{39}Ar$ age spectra for seven groundmass and/or plagioclase analyses from dredges D42 and D44. The $^{40}Ar/^{39}Ar$ ages are weighted age estimates with errors reported at the 95% confidence level, including 0.15% standard deviations in the J-value. All samples were monitored against FCT-NM sanidine (28.201 ± 0.023 Ma, 1σ) as calibrated by *Kuiper et al.* [2008]. Data are listed in the supporting information and ArArCALC age calculation files can be downloaded from the EarthRef.org Digital Archive (ERDA).

ST101 getter operated at 400°C and two SAES Fe-V-Zr ST172 getters operated at 200°C and room temperature, respectively.

All ages were calculated using the corrected *Steiger and Jäger* [1977] decay constant of $5.530 \pm 0.097 \times 10^{-10}$ 1/yr (2σ) as reported by *Min et al.* [2000]. Incremental heating plateau ages and isochron ages were calculated as weighted means with $1/\sigma^2$ as weighting factor [*Taylor*, 1997] and as YORK2 least-square fits with correlated errors [*York*, 1968] using the ArArCALC v2.6.2 software from *Koppers* [2002] available from the http://earthref.org/ArArCALC/website.

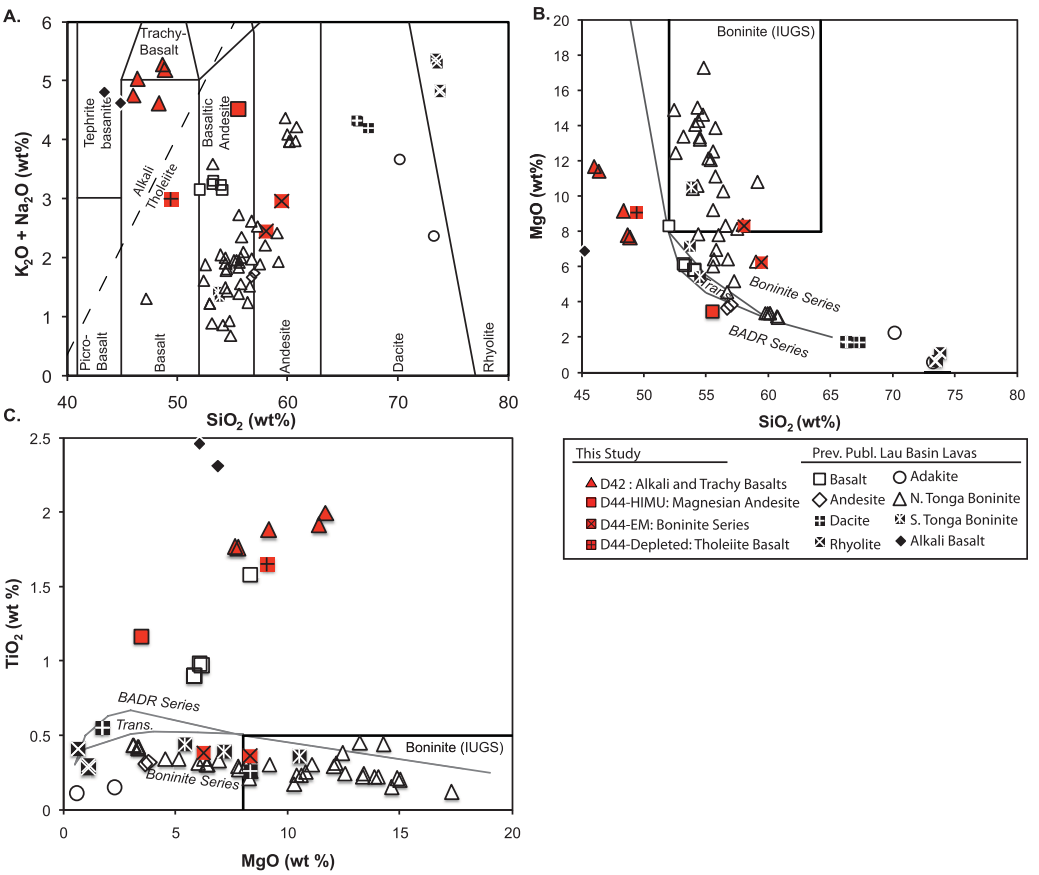

Figure 3. Silica versus total alkali plot, with subdivisions for different rock classifications based on *Le Bas et al.* [1986]. The alkali-tholeiite line is from *Macdonald and Katsura* [1964]. The boninite fields are defined by the IUGS *Le Bas* [2000]. The line dividing the boninite series from the basalt-andesite-dacite-rhyolite (BADR) series is from *Pearce and Robinson* [2010] (trans. = transitional). Previously published Lau Basin data are from *Falloon and Crawford* [1991]; *Danyushevsky et al.* [1995]; *Falloon et al.* [2007, 2008]; *Cooper et al.* [2010]; and *Resing et al.* [2011].

3. Results

3.1. Major Element Compositions

In a silica versus total alkali diagram, all lavas from dredge D42 are alkalic, and plot in either the field for alkali basalts or trachy basalts [*Macdonald and Katsura*, 1964] (Figure 3). Alkali basalts were reported previously in the NELB approximately 60 km northeast of dredge D42 [*Falloon et al*., 2007; *Zlobin et al*., 1991].

The samples from dredge D44 cover a wide range of compositions. Sample D44-91 is a basaltic tholeiite. Sample D44-46 plots in the boninite field (Figure 3), while sample D44-38 is part of the boninite series and is likely a boninite differentiate. This complements the detection of other boninites in the NELB [*Falloon et al*., 1987; *Falloon and Crawford*, 1991; *Sobolev and Danyushevsky*, 1994; *Danyushevsky et al*., 1995; *Falloon et al*., 2007, 2008; *Resing et al*., 2011] and documents the existence of boninitic lavas ~200 km to the west of these prior discoveries (Figure 1). The final dredge D44 sample, D44-26, is a magnesian andesite with adakitic characteristics. This sample has geochemical characteristics that are consistent with an adakitic composition, including Al_2O_3 >15 wt. %, MgO > 3 wt. %, and Sr > 400 ppm [*Castillo*, 2012]. However, while true adakites have been identified previously in the NELB [*Falloon et al*., 2008], D44-26 is not a true adakite as the SiO_2 is slightly lower (< 56 wt. %), and the Y concentration is slightly higher (> 18 ppm) than suggested for adakites [e.g., *Castillo*, 2012].

3.2. Trace Element Compositions

The primitive mantle-normalized trace element patterns for dredge D42 whole rocks are all relatively similar and exhibit incompatible trace element enrichment (Figure 4), an observation consistent with their alkali

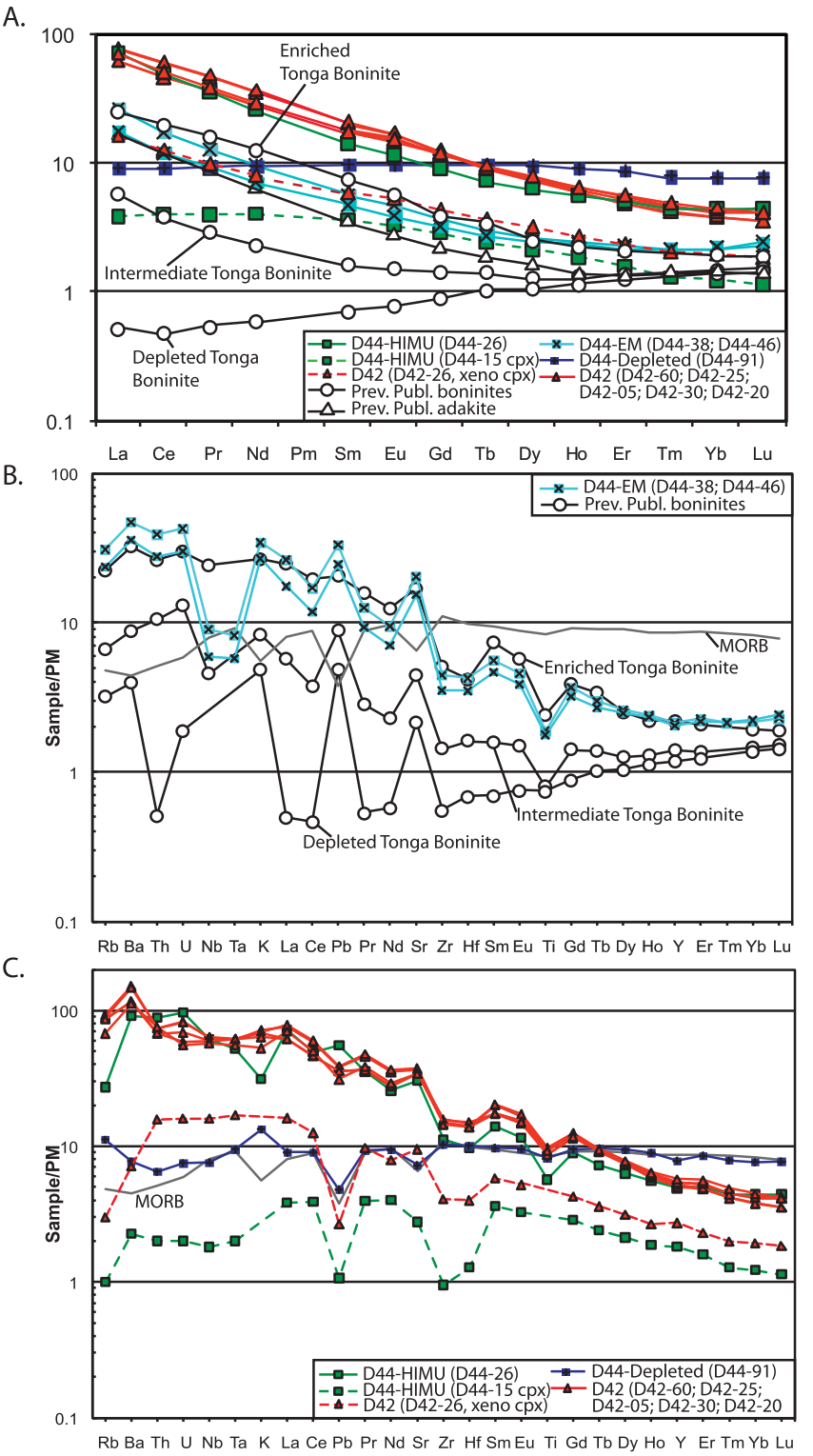

Figure 4. Primitive mantle-normalized trace element patterns for the lavas examined in this study. The primitive mantle composition is from *McDonough and Sun* [1995]. All trace element data used in this plot, including data used to construct the data fields, were measured by ICP-MS. All trace element variation diagrams represent whole rock measurements of lavas, except for sample D44-15, which represents trace element measurements of clinopyroxene, and D42-26, which represents trace element measurements of clinopyroxene separated from an olivine websterite xenolith. Three types of boninites, Tongan enriched, intermediate, and depleted, are defined by *Falloon et al.* [2007]. A Tongan adakite, sample 113-2-12 from *Falloon et al.* [2007], is also added for reference.

and trachy basalt designations. The trace element pattern exhibits notable depletions in Zr, Hf, and Ti and slight depletions in Nb and Ta.

Dredge D44 whole rock lavas show greater diversity in primitive mantle-normalized trace element patterns. The most incompatible element-enriched lava from dredge D44 (D44-HIMU; see in section 3.3) is a magnesian andesite (with adakitic characteristics) that is depleted in Ti, Zr, Hf, Nb, and Ta and enriched in Pb. The two boninite series lavas (classified as part of the D44-EM group, see section 3.3) are also relatively enriched in incompatible elements and display striking depletions in Ti, Nb, Ta, Zr, and Hf and prominent enrichments in Sr and Pb. Based on their trace element characteristics, *Falloon et al*. [2007] defined three types of boninites in the NELB: depleted, intermediate, and enriched (Figure 4). The two new boninite series lavas from dredge D44 have primitive mantle-normalized trace element patterns that are most similar to the enriched boninites from *Falloon et al*. [2007]. However, the new boninite series lavas show some features that are similar to the intermediate boninites from *Falloon et al*. [2007], including greater depletions in Nb and a slight U-shaped pattern in the primitive mantle-normalized rare earth element diagram (i.e., primitive mantle-normalized Lu/Yb >1). In contrast, the basaltic tholeiite (D44-depleted in section 3.3) has a pattern relatively similar to average global MORB [*Gale et al*., 2013].

3.3. Hf-Pb-Sr-Nd Isotopic Compositions

Supporting information Figures S1 and S2 provide a comparison of the isotopic data for the new samples with previously published isotopic data for lavas from the Lau Basin. In comparison to other lavas from the Lau Basin, a subset of the new NELB lavas exhibits extreme geochemical compositions. When compared to all other lavas from the nearby Tonga Arc as well as the Eastern Lau Spreading Center (ELSC), Central Lau Spreading Center (CLSC), and Fonualei Rift (FRSC), all of our new samples (with the exception of the D44-depleted sample) are more geochemically enriched, with lower $^{143}Nd/^{144}Nd$ and higher $^{87}Sr/^{86}Sr$ (supporting information Figure S1). The new lavas in this study extend to isotopic compositions that overlap with previously described lavas from the NELB [*Falloon et al*., 2007, 2008]. The dredge D42, dredge D44-EM, and dredge D44-HIMU lavas also show more radiogenic Pb isotopic ratios than samples from the nearby Niuafo'ou Island and Rochambeau Rifts, but are similar to (and, in some cases, more radiogenic than) Pb isotopic compositions previously reported from the NELB [*Falloon et al*., 2007, 2008].

Dredge D42 alkalic lavas have relatively radiogenic Pb isotope compositions ($^{206}Pb/^{204}Pb$ up to 19.162, $^{207}Pb/^{204}Pb$ of 15.643, and $^{208}Pb/^{204}Pb$ of 39.177), which are slightly lower than a subset of lavas from dredge D44 (see below) (Figures 5 and 6). The dredge D42 lavas also have low $^{143}Nd/^{144}Nd$ (down to 0.512697). When plotted in $^{143}Nd/^{144}Nd$ versus $^{176}Hf/^{177}Hf$ space, the dredge D42 samples fall along the mantle array, with $^{176}Hf/^{177}Hf$ ranging from 0.282909 to 0.282968 (Figure 5b). $^{87}Sr/^{86}Sr$ ratios are relatively high (up to 0.704233) in the dredge D42 lavas, but higher values have previously been observed in the northern Lau Basin for alkali basalts (up to 0.704299), boninites (up to 0.704884) and adakites (up to 0.705655) [*Falloon et al*., 2007, 2008]. In all other isotopic spaces, the dredge D42 lavas plot near previously published alkali basalts from the northern Lau Basin from *Falloon et al*. [2007] (Figures 5 and 6). Clinopyroxene from the olivine websterite xenolith, sample D42-26, is isotopically similar to whole rock lavas from the same dredge, but shifted toward slightly lower $^{87}Sr/^{86}Sr$ (Table 2). It is worth noting that while the dredge D42 lavas have relatively homogenous isotopic compositions, the variability in Sr, Nd, Hf, and Pb isotopic compositions suggests that the dredge samples multiple different flows.

Dredge D44 lavas are isotopically more heterogeneous than lavas from dredge D42 and are divided into three isotopic groups based on their geochemical signatures. The first group, D44-HIMU, has the highest $^{206}Pb/^{204}Pb$, $^{207}Pb/^{204}Pb$, and $^{208}Pb/^{204}Pb$ so far observed in the Lau Basin (19.580, 15.664, and 39.413, respectively) (Figure 5). While the D44-HIMU samples do not show extreme HIMU signatures, they extend toward an extreme HIMU component (see section 4.2). This isotopic group includes a lava with a magnesian andesite composition (D44-26). The dredge D44 clinopyroxene separate, sample D44-15, is included in the D44-HIMU group as it is isotopically similar to the magnesian andesite, but is shifted to slightly lower Pb isotopic values. The D44-HIMU samples also exhibit high $^{87}Sr/^{86}Sr$ (up to 0.704087) and relatively low $^{143}Nd/^{144}Nd$ (down to 0.512778) (Figure 5a). Only one whole rock sample in the D44-HIMU group, sample D44-26, was measured for its Hf isotopic composition (0.282991), and is similar to that found in dredge D42; this lava plots close to the dredge D42 samples in $^{143}Nd/^{144}Nd$–$^{176}Hf/^{177}Hf$ space (Figures 5 and 6).

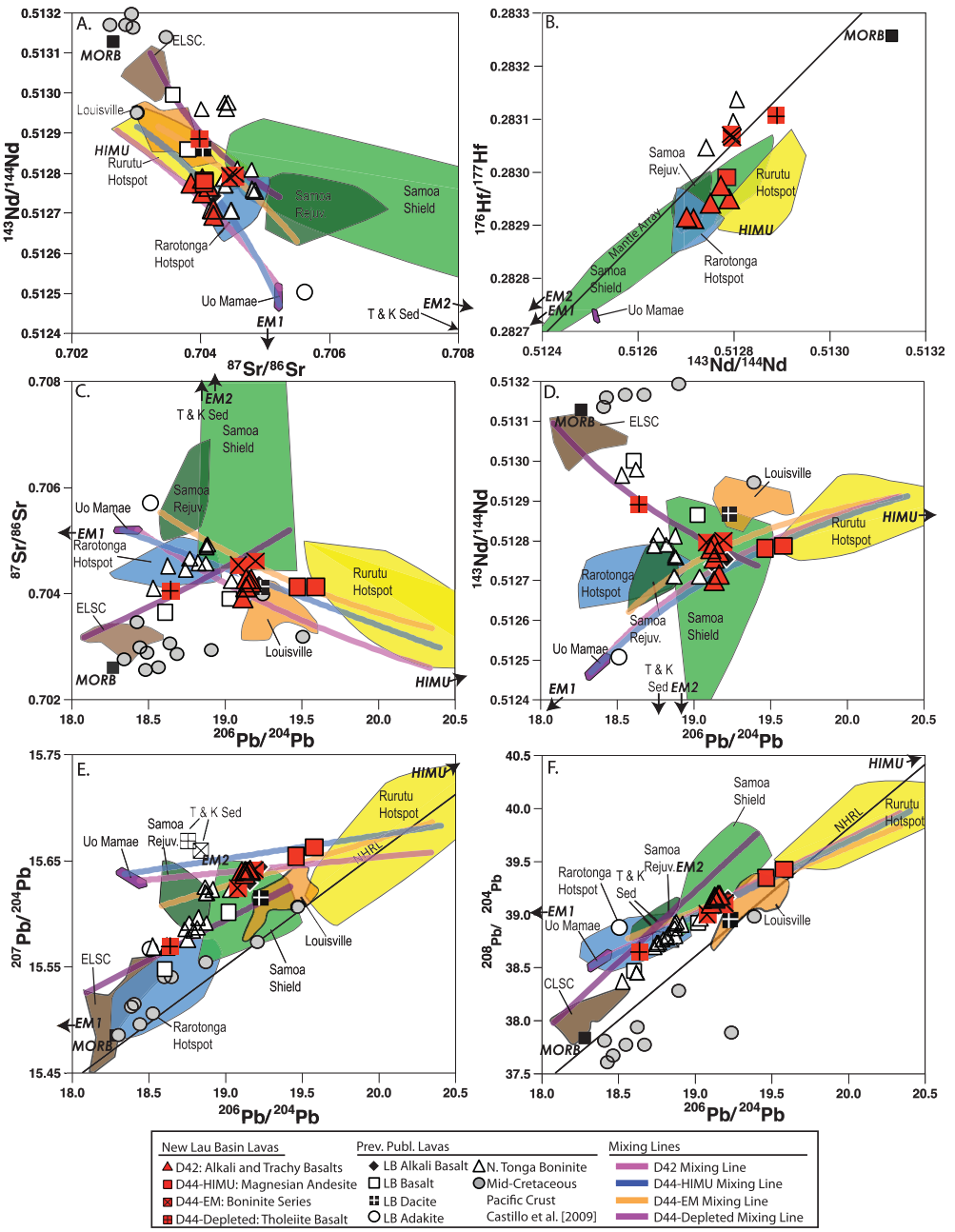

Figure 5. Sr, Nd, Hf, and Pb isotopic relationships among new lavas dredged from the NELB and lavas from the Samoan hotspot, Rurutu hotspot, Rarotonga hotspot, and Louisville hotspot. In addition to the new data from the NELB (plotted as various red symbols), previously published whole rock NELB data are from *Falloon and Crawford* [1991]; *Danyushevsky et al.* [1995]; *Falloon et al.* [2007, 2008]; and *Caulfield et al.* [2012]. LB stands for Lau Basin. Data from bulk composition of sediment columns taken from outboard of the Tonga and Kermadec Trenches (T&K) are included when available [*Plank and Langmuir*, 1998]. Pacific crustal material from outboard of the Tonga Trench is from *Castillo et al.* [2009]. (b) A line representing the mantle array is from *Vervoort et al.* [1999], defined as $\varepsilon_{Hf} = 1.33*\varepsilon_{Nd} + 3.19$. The Northern Hemisphere reference line (NHRL) from *Hart* [1984] is shown in Figures 5e and 5f. Abbreviations: MORB *mid-ocean ridge basalt;* ELSC *Eastern Lau Spreading Center*. Data for the ELSC are from *Hergt and Woodhead* [2007] and *Escrig et al.* [2009]. Values for Samoan data fields are from *Wright and White* [1987]; *Poreda and Craig* [1992]; *Workman et al.* [2004]; *Workman and Hart* [2005]; *Jackson et al.* [2007a, 2007b, 2010]; *Salters et al.* [2011]. Uo Mamae data are from *Pearce et al.* [2007]; *Regelous et al.* [2008]. Rurutu hotspot data, which include lavas from the young series of Arago Seamount, the young series of Rurutu Island, Mauke Island, and Atiu Island, are from *Nakamura and Tatsumoto* [1988]; *Chauvel et al.* [1992]; *Hauri and Hart* [1993]; *Hemond et al.* [1994]; *Woodhead* [1996]; *Chauvel et al.* [1997]; *Kogiso et al.* [1997]; *Salters and White* [1998]; *Schiano et al.* [2001]; *Lassiter et al.* [2003]; *Bonneville et al.* [2006]; *Salters et al.* [2011]; *Hanyu et al.* [2011]. Rurutu sample 74-394 from *Chauvel et al.* [1997] is excluded from this field; *Chauvel et al.* [1997] ignored this sample due to its unusual geochemistry and we note that it is a cobble of unknown origin. Rarotonga data are from *Nakamura and Tatsumoto* [1988]; *Hauri and Hart* [1993]; *Salters and White* [1998]; *Schiano et al.* [2001]; *Thompson et al.* [2001]; *Salters et al.* [2011]; *Hanyu et al.* [2011]. Louisville data are from *Cheng et al.* [1987]; *Beier et al.* [2011]; *Vanderkluysen et al.* [2014]. Louisville samples identified as highly altered or very highly altered were excluded. The MORB average is from *Su* [2003].

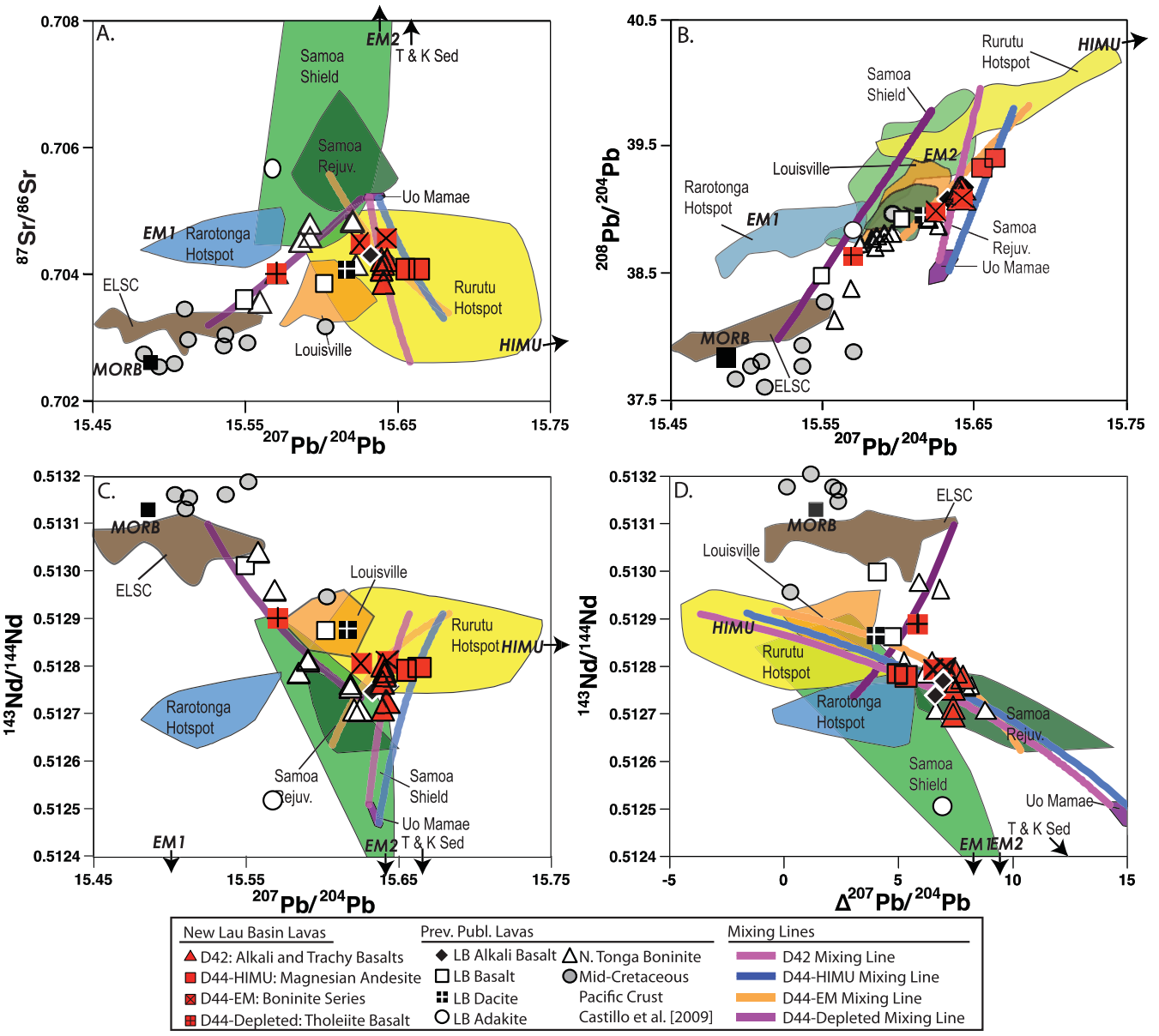

Figure 6. Sr, Nd, and Pb isotopic relationships among new lavas dredged from the Lau Basin and lavas from the Samoan hotspot, Rurutu hotspot, Rarotonga hotspot, and Louisville hotspot. Abbreviations and data sources same as Figure 5. $\Delta^{207}Pb/^{204}Pb$ and $\Delta^{208}Pb/^{204}Pb$ are defined in *Hart* [1984] the following way: $\Delta^{207}Pb/^{204}Pb = 0.1084(^{207}Pb/^{204}Pb) + 13.491$, and $\Delta^{208}Pb/^{204}Pb = 1.209(^{208}Pb/^{204}Pb) + 15.627$.

The second group of dredge D44 lavas, designated D44-EM, lies within the boninitic series in Figure 4 and has the most geochemically enriched Sr isotopic compositions (up to 0.704564) of all lavas from dredge D44. In a plot of $^{87}Sr/^{86}Sr$ versus $^{143}Nd/^{144}Nd$ (Figure 5a), the D44-EM lavas overlap with the range of compositions previously published from NELB boninites. The corresponding $^{143}Nd/^{144}Nd$ (ranging from 0.512793 to 0.512798) and $^{176}Hf/^{177}Hf$ (ranging from 0.283071 to 0.283073) are slightly higher than values measured in dredge D42 and D44-HIMU lavas (Figure 5b). The D44-EM lavas plot slightly above the mantle array in $^{143}Nd/^{144}Nd$–$^{176}Hf/^{177}Hf$ space. D44-EM lavas also have relatively radiogenic Pb isotopic ratios ($^{206}Pb/^{204}Pb$ up to 19.190, $^{207}Pb/^{204}Pb$ of 15.642, and $^{208}Pb/^{204}Pb$ of 39.095), but these values are not as radiogenic as those found in the D44-HIMU lavas.

The last geochemical group in dredge D44, termed D44-depleted, consists of a single tholeiitic basalt sample (sample D44-91), which has the highest $^{143}Nd/^{144}Nd$ (0.512889) of any lava in the new data set. The

most salient observation regarding this sample is that it has high $^{3}He/^{4}He$ (19.3 Ra), which exceeds the $^{3}He/^{4}He$ measured in all the other lavas from dredges D42 and D44 (see below). In most isotopic spaces, the D44-depleted lava plots within the field representing Rochambeau Bank and Rochambeau Rift lavas (supporting information Figures S1 and S2), which were previously found to exhibit high $^{3}He/^{4}He$ (up to 28.1 Ra) [*Lupton et al*., 2009]. However, in some isotopic spaces (e.g., $^{206}Pb/^{204}Pb$ versus $^{207}Pb/^{204}Pb$ and $^{143}Nd/^{144}Nd$ versus $^{176}Hf/^{177}Hf$), the D44-depleted lava plots outside the field of Rochambeau lavas and thus expands the field in radiogenic isotope space that encompasses high $^{3}He/^{4}He$ lavas from the Lau Basin region.

3.4. Helium Isotopic Compositions

The highest $^{3}He/^{4}He$ value measured in this study for sample D44-91 is 19.3 Ra. The other samples have $^{3}He/^{4}He$ between 2.8 and 8.5 Ra (Figure 7a). Two samples (both glass) from dredge D42 have $^{3}He/^{4}He < 3.8$ Ra, while a third sample (olivine) from dredge D42 with higher ^{4}He concentrations has higher $^{3}He/^{4}He$ (7.9 Ra). However, all three dredge D42 lavas with $^{3}He/^{4}He$ measurements have similar Sr, Nd, Hf, and Pb isotopic compositions, and it is therefore reasonable to assume that the primary magmatic $^{3}He/^{4}He$ may also have been similar. Thus, the lower $^{3}He/^{4}He$ in these two glasses from dredge D42 lavas may relate to their lower ^{4}He, which can make a lava more susceptible to reduction of $^{3}He/^{4}He$ either by atmospheric contamination or addition of radiogenic ^{4}He [e.g., *Zindler and Hart*, 1986; *Hilton et al*., 1993]. The D44-EM boninite series lavas all have $^{3}He/^{4}He$ of $\sim$8 Ra (Figure 8a). The D44-HIMU lavas have $^{3}He/^{4}He$ from 7.8 Ra (the magnesian andesite) to 7.7 Ra. The $^{3}He/^{4}He$ and heavy radiogenic isotopic compositions are shown in Figures 7b–7d.

3.5. $^{40}Ar/^{39}Ar$ Age Dates

Four dredge D42 lavas have been $^{40}Ar/^{39}Ar$ age dated by incremental heating of groundmass phases. The ages range from 364.8 ± 3.7 ka to 1.223 ± 0.019 Ma (2σ) and exhibit relatively flat and wide age plateaus (Figure 2). Internal reproducibilities are consistent with concordant plateau, inverse isochron, and total fusion ages at the 2σ confidence level, allowing the groundmass ages to be interpreted as eruption ages [e.g., *Koppers et al*., 2000]. Isochron $^{40}Ar/^{36}Ar$ intercepts are consistent with a trapped argon component similar to an atmospheric argon composition of 295.5 (Table 4). The observed 0.36–1.22 Ma age range is consistent with expected longevities for the construction of single intraplate volcanoes [e.g., *Konter et al*., 2009; *Koppers et al*., 2011; *Clague and Sherrod*, 2014]. Unfortunately, only one sample (D42-60) has both ages and geochemical data as the geochemical, isotopic, and geochronological analyses require samples with dissimilar characteristics. For example, samples targeted for $^{3}He/^{4}He$ analysis generally require higher MgO (and abundant phenocrysts of olivine or pyroxene) than rocks targeted for $^{40}Ar/^{39}Ar$ dating, which generally should be more evolved (lower MgO) so as to have higher K and modal plagioclase abundances.

Two dredge D44 samples were dated by incrementally heating their phenocrystic plagioclase phases, providing reproducible plateau ages of 1.249 ± 0.051 Ma (sample D44-08) and 1.279 ± 0.115 Ma (2σ) (sample D44-26) (Figure 2). The groundmass sample D44-12, however, yielded a complex age pattern due to ^{39}Ar recoil acting on very fine-grained alteration that may remain in the dated groundmass separates, even following an extensive acid-leaching protocol [e.g., *Koppers et al*., 2000, 2011]. Assuming internal redistribution of ^{39}Ar during the recoil process, the total fusion age (1.536 ± 0.030 Ma) of sample D44-12 may be viewed as a reasonable indicator for its eruption age, which is only slightly older than the two concordant plagioclase ages of samples D44-08 and D44-26. Only one sample (D44-26) from the D44-HIMU group (a magnesian andesite) has both geochemical and age data.

4. Discussion

4.1. Tectonic and Isotopic Constraints on Hotspot Components in the Northern Lau Basin

A number of hotspots have been suggested to contribute geochemical signatures to the Lau Basin. The Louisville hotspot and the older segments of hotspot trails emerging from the Cook-Austral volcanic chain (along with their volcaniclastic aprons) have been subducted into the Tonga Trench, potentially imparting distinct geochemical signatures to lavas from the Lau Basin [e.g., *Turner and Hawkesworth*, 1998; *Ewart et al*., 1998; *Falloon et al*., 2007; *Regelous et al*., 2010]. In contrast, the presence of a Samoan hotspot component is

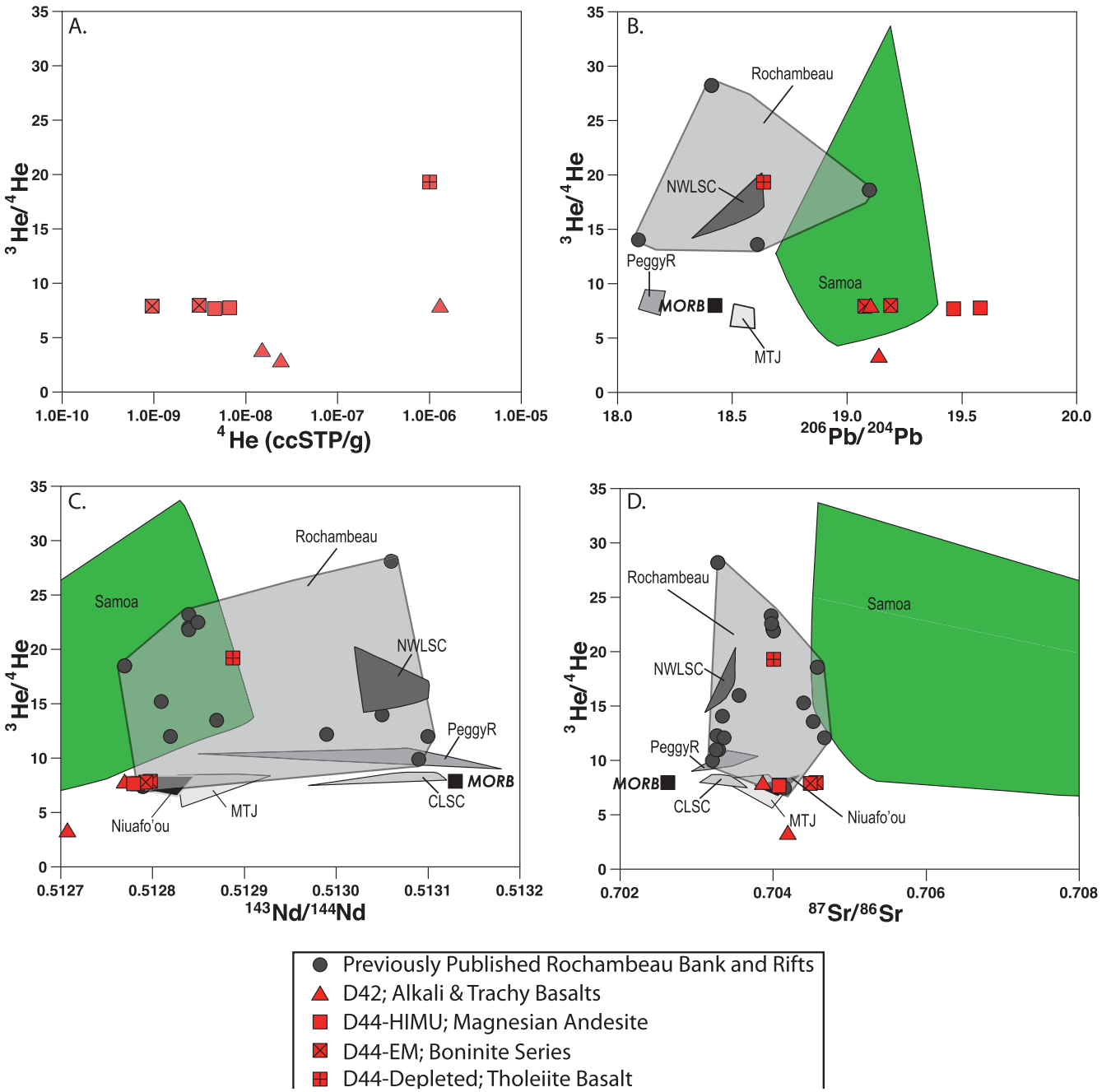

Figure 7. Helium isotopic data for samples from the NELB plotted against their respective gas concentrations and Pb-Sr-Nd isotopic ratios. Note that one dredge D42 sample has $^3He/^4He$, but no other isotopic data. The three lavas with $^3He/^4He$ from dredge D42 span a wide range of $^3He/^4He$: The much lower $^3He/^4He$ in two dredge D42 lavas may relate to their lower ^4He concentrations, which potentially render a lava more susceptible to reduction of $^3He/^4He$ [e.g., *Hilton et al*., 1993]. However, four other samples from D44-HIMU and D44-EM have even lower helium concentrations ($<6.7 \times 10^{-9}$ ^4He cc STP/g), but still show MORB-like $^3He/^4He$ ratios ranging from 7.7 to 8 Ra. Grey circles represent previously published Rochambeau Bank and Rift data and are plotted separately as some lavas have extremely high $^3He/^4He$. Abbreviations: NWLSC *Northwest Lau Spreading Center*; MTJ = *Mangatolu Triple Junction*; CLSC = *Central Lau Spreading Center*, Peggy R = *Peggy Ridge*. Samoan data are from *Farley et al*. [1992]; *Workman et al*. [2004]; *Jackson et al*. [2007a, 2007b, 2014]. Rochambeau Bank and Rift data are from *Volpe et al*. [1988]; *Poreda and Craig* [1992]; *Lupton et al*. [2009]; *Tian et al*. [2011]; *Hahm et al*. [2012]; *Lytle et al*. [2012]. Mangatolu Triple Junction data are from *Hilton et al*. [1993]; *Honda et al*. [1993]; *Regelous et al*. [2008]; *Tian et al*. [2011]; *Hahm et al*. [2012]. NWLSC data are from *Lupton et al*. [2009]; *Lytle et al*. [2012]. Peggy Ridge and northeast of Peggy Ridge data are from *Volpe et al*. [1988]; *Tian et al*. [2008]; *Hahm et al*. [2012]; *Price et al*. [2014]. Niuafo'ou data are from several sources *Volpe et al*. [1988]; *Poreda and Craig* [1992]; *Hahm et al*. [2012].

unlikely to be introduced by subduction, but instead is hypothesized to be incorporated in the Lau Basin mantle region via toroidal flow around the downgoing Tonga slab [e.g., *Druken et al*., 2014; *Price et al*., 2014]. In this section, we evaluate whether seamounts from the Cook-Austral volcanic chain and the

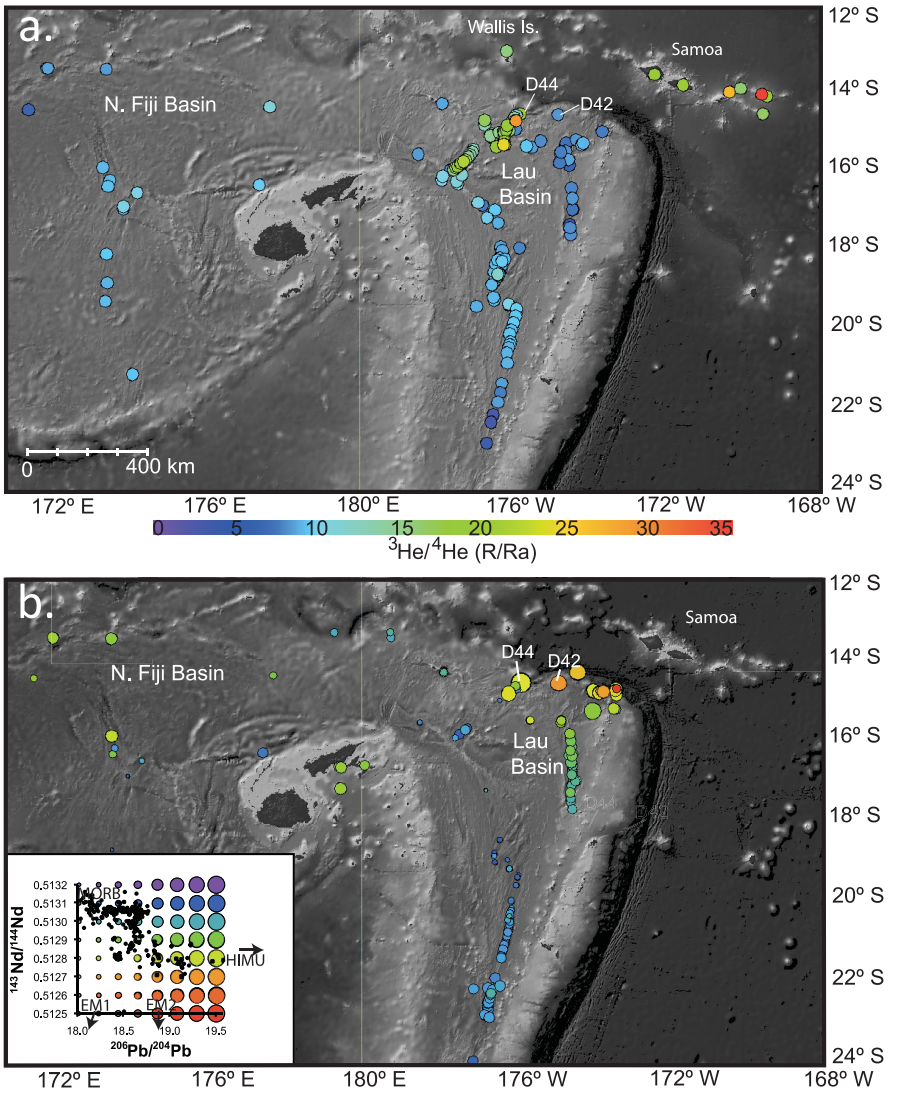

Figure 8. Maps of the Lau and North Fiji Basins showing distribution of new and previously published He, Nd, and Pb isotopic data. (a) $^{3}He/^{4}He$ from new lavas and previously published lavas from the region, and includes data from Samoa (only the highest $^{3}He/^{4}He$ found on each Samoan island is shown). He isotopic data are from *Poreda and Craig* [1992]; *Hilton et al*. [1993]; *Honda et al*. [1993]; *Nishio et al.* [1998]; *Workman et al*. [2004]; *Jackson et al.* [2007a, 2007b]; *Lupton et al.* [2009]; *Hahm et al*. [2012]; *Price et al.* [2014]. (b) The relationship between Pb and Nd isotopic data in the Lau and North Fiji Basins (data from the Tonga Arc are not shown, but young (<3 Ma) ocean island basalt-type lavas from Fiji have been included). Data shown in the inset of the lower panel are the same geochemical data shown on the map. Pb and Nd isotopic data are from: *Gill* [1984]; *Loock* [1990]; *Nohara et al.* [1994]; *Peate et al*. [1997]; *Fretzdorff et al.* [2006]; *Pearce et al*. [2007]; *Falloon et al.* [2007]; *Hergt and Woodhead* [2007]; *Regelous et al.* [2008]; *Escrig et al*. [2009]; *Haase et al.* [2009]; *Escrig et al.* [2012]; *Lytle et al*. [2012]; *Timm et al.* [2013]; *Price et al*. [2014]. Data for Samoan lavas are not shown in the bottom plot because the extreme low $^{143}Nd/^{144}Nd$ values in Samoa skew the color distribution used to contour the Nd isotopic data in the Lau Basin. Base maps were created using GeoMapApp (http://www.geomapapp.org) with topographic and bathymetric data from SRTM_PLUS [*Becker et al*., 2009].

Louisville hotspot are likely to influence the geochemistry of NELB lavas, and whether any signatures from the nearby Samoan plume source are detected in the NELB.

4.1.1. The Three Hotspots of the Cook-Austral Volcanic Lineament

The Cook-Austral volcanic lineament is suggested to be comprised of three distinct, age-progressive hotspot tracks [e.g., *Duncan and McDougall* 1976; *Turner and Jarrard*, 1982; *Matsuda et al.*,1984; *Diraison*, 1991; *Chauvel et al*., 1997; *McNutt et al*.,1997; *Bonneville et al*., 2002; *Bonneville et al*., 2006; *Konter et al*., 2008; *Maury et al*., 2013]. Like Hawaii (also situated on the Pacific Plate), each of the three Cook-Austral hotspots is anchored by a relatively young volcanic island or seamount on its eastern terminus: Macdonald seamount

anchors the "Macdonald hotspot" track [*Diraison*, 1991], Arago seamount anchors the "Rurutu hotspot" track [*Bonneville et al*., 2002], and Rarotonga Island anchors the "Rarotonga hotspot" track (Figure 1). Each of the three hotspots is argued to be long-lived and geochemically continuous back to the Cretaceous [*Staudigel et al*., 1991; *Koppers et al*., 1998, 2003, 2007; *Konter et al*., 2008]. While the individual paths of each of the hotspot tracks are not currently fully constrained and mapped out, they can be predicted through the use of absolute plate motion models that are anchored to the proposed location of currently active (or recent) volcanism at each hotspot. Pacific Plate reconstructions following the *Wessel and Kroenke* [2008] model show that the Tokelau Islands, the Gilbert Ridge, and the Western Pacific Seamount Province (WPSP) may represent the older, Cretaceous portions of the Macdonald, Rurutu, and Rarotonga seamounts, respectively (Figure 1).

Macdonald hotspot: Using lavas from Tubuai Island (from the Macdonald hotspot track) as a proxy for HIMU volcanoes of the Cook-Austral volcanic lineament, *Falloon et al*. [2007] suggested that subducted HIMU Cook-Austral seamounts may be at the origin of the radiogenic Pb isotope compositions in NELB lavas. However, the *Wessel and Kroenke* [2008] reconstruction for the Macdonald hotspot track does not intersect the Tonga Trench at any point in time (Figure 1). As a result, the geochemical components in the Lau Basin are unlikely to include a contribution from the Macdonald hotspot. Therefore, it is necessary to evaluate an alternative model for the origin of the HIMU signature in the NELB.

Rurutu hotspot: Based on the *Wessel and Kroenke* [2008] reconstruction (Figure 1), the trace of the Rurutu hotspot "grazes" the northern tip of the Tonga Trench. Considering the fact that there are no other known candidate hotspots in the region likely to contribute a HIMU signature of the magnitude observed in the NELB lavas, we suggest that portions of the Rurutu hotspot trail or volcaniclastic aprons found around Rurutu volcanoes subducted into the Tonga Trench and added a HIMU component to mantle sources in the NELB (Figure 1 and below). However, the origin of the EM1 signature in the Lau Basin requires explanation.

Rarotonga hotspot: The youngest proposed hotspot in the Cook-Austral volcanic lineament, the Rarotonga hotspot, is located ~1500 km east of the Tonga Trench. A *Wessel and Kroenke* [2008] plate reconstruction anchored to Rarotonga Island shows that a portion of an older segment of the Rarotonga hotspot track may have subducted into the Tonga Trench and beneath the NELB (Figure 1). The plate reconstruction suggests that Rarotonga hotspot-related seamounts older than 15 Ma could have been subducted into the Tonga Trench. However, not all of the older (i.e., older than 15 Ma) Rarotonga seamounts were subducted into the Tonga Trench, as the portion of the Rarotonga hotspot track older than 30 Ma extends north of the Vitiaz Lineament to the WPSP on the Pacific Plate (Figure 1). Therefore, the Rarotonga hotspot is likely to impart an EM1 geochemical pedigree [*Konter et al*., 2008; *Konter and Jackson*, 2012] to the NELB via subduction of 15–30 Ma Rarotonga hotspot-related seamounts beneath the northeastern region of the back-arc basin.

The Rarotonga hotspot also may have imparted an EM1 signature on the Pacific lithosphere [*Konter and Jackson*, 2012] or formed an EM1-flavored "keel" attached to the Pacific lithosphere, when the Pacific Plate passed over the Rarotonga hotspot at ~15 Ma (Figure 1). Plate motion "rafted" this keel to its current location in the Samoan region, giving rejuvenated Samoan volcanism an EM1 signature (distinct from the shield stage of volcanism at the Samoan hotspot) that has geochemical affinities with hotspot volcanism from Rarotonga [*Wright and White*, 1987; *Workman et al*., 2004; *Konter and Jackson*, 2012]. Uo Mamae, a seamount (0.94 Ma) [*Hawkins and Natland*, 1975] located 100 km to the south of the axis of the Samoan hotspot, lies on the reconstructed track of Rarotonga and has lavas with even more extreme EM1 signatures than Samoan rejuvenated lavas [*Pearce et al*., 2007; *Falloon et al*., 2007; *Regelous et al*., 2008]. Rejuvenated volcanism at Uo Mamae lavas may have been triggered by tectonic stresses as Uo Mamae (located just 30 km outboard of the trench; Figure 1) is subducted into the Tonga Trench. A similar type of tectonically-triggered rejuvenated volcanism was suggested for the nearby Samoan island of Savai'i, located ~130 km from the Tonga Trench, as the island has been almost completely resurfaced with rejuvenated volcanism [*Hawkins and Natland*, 1975; *Konter and Jackson*, 2012] that overlays older, shield-stage volcanism [*Koppers et al*., 2008, 2011]. The pervasive EM1 signature in young Samoan lavas therefore may ultimately be a geochemical signal that has an origin at the Rarotonga hotspot [*Konter and Jackson*, 2012]. When volcanoes from the Rarotonga hotspot (like Uo Mamae) are subducted, their EM-1 geochemical signatures are communicated to back-arc lavas in the NELB.

One potential weakness with this model is that the proposed Rarotonga hotspot consists of only a single volcano with an age of 1.1–2.3 Ma (Rarotonga Island) [*Turner and Jarrard*, 1982; *Matsuda et al*., 1984]. While young (0.74–1.93 Ma) [*Turner and Jarrard*, 1982], rejuvenated lavas on Aitutaki Island may be linked to the Rarotonga hotspot [e.g., *Chauvel et al*., 1997; *Maury et al*., 2013], much of this hotspot track remains unsampled. If indeed the Cretaceous volcanic edifices in the WPSP formed over the Rarotonga hotspot prior to 90 Ma [*Koppers et al*., 1998, 2003; *Konter et al*., 2008], then approximately 90 Myr of Rarotonga hotspot volcanism—between the WPSP and Rarotonga-Aitutaki—remains undiscovered and unsampled. Compared to the whole Cook-Austral volcanic lineament, the trace of the Rarotonga (and Rurutu, discussed above) hotspot is less prominent in the region between Rarotonga Island and the Tonga Trench. There are scattered seamounts and atolls along the expected track of Rarotonga (and Rurutu) hotspot outboard of the Tonga trench. Future dredging campaigns are needed to evaluate whether these volcanic features relate to the Rarotonga (and the Rurutu) hotspot. Nonetheless, the existing body of geochemical, geochronological, and plate motion evidence in the region is consistent with the trace of the Rarotonga hotspot being subducted into the northernmost region of the Tonga Trench. Therefore, we argue that subduction of the Rarotonga hotspot material provides a plausible model for the origin of the EMI signatures found in the Lau Basin (see section 4.2 below).

4.1.2. The Louisville Hotspot

In some isotopic spaces (Figures 5 and 6), the samples from D44-HIMU, D44-EM, and dredge D42 plot in or near the Louisville field. Therefore, an important question is whether the subducted Louisville hotspot has contributed to the geochemical diversity observed in the NELB. The Louisville hotspot exhibits relatively high $^{206}Pb/^{204}Pb$ (up to 19.606) and has been suggested to contribute to the elevated Pb isotopic compositions observed in a subset of volcanoes from the Tonga arc. However, Louisville lavas have $^{207}Pb/^{204}Pb$ and $^{208}Pb/^{204}Pb$ compositions (not age-corrected) that are lower than the NELB lavas with the most radiogenic Pb isotopic signatures (i.e., D44-HIMU lavas) and, therefore, cannot have contributed the extreme HIMU signature found in the NELB (Figures 5 and 6) [*Cheng et al*., 1987; *Beier et al*., 2011; *Vanderkluysen et al*., 2014] (see supporting information Discussion).

In addition, the Louisville hotspot cannot account for the enriched mantle (high $^{87}Sr/^{86}Sr$) values in the D44-EM lavas. While Louisville does have $^{87}Sr/^{86}Sr$ that extends up to 0.70421 [*Vanderkluysen et al*., 2014], the NELB lavas with the highest $^{87}Sr/^{86}Sr$ (D44-EM and dredge D42) require even higher $^{87}Sr/^{86}Sr$ (0.704564) than observed in the Louisville chain. Furthermore, Louisville hotspot lavas cannot explain the high $^{3}He/^{4}He$ component of 19.3 Ra observed in NELB lavas as Louisville $^{3}He/^{4}He$ extends to only 10.6 Ra [*Hanyu*, 2014]. It is notable that Louisville has been subducting into the northern Lau Basin for the past 4 Ma, and the intersection between the Louisville hotspot and the Tonga Trench has swept from north to south over this time interval. Therefore, Louisville is no longer being subducted into the northern Lau Basin, and the Louisville hotspot track now intersects with the trench ~1200 km south of the northern terminus of the Tonga trench. This is much too far to the south for Louisville to contribute geochemical signatures to the young (<1.3 Ma) NELB lavas.

4.1.3. The Samoan Hotspot

A Samoan plume component has been suggested to influence the geochemistry of the mantle underlying the Lau Basin [e.g., *Volpe et al*., 1988; *Poreda and Craig*, 1992; *Wendt et al*., 1997; *Ewart et al*., 1998; *Tian et al*., 2008; *Lupton et al*., 2009; *Tian et al*., 2011; *Hahm et al*., 2012; *Lupton et al*., 2012a, 2012b; *Lytle et al*., 2012; *Price et al*., 2014]. While components from the Rurutu and Rarotonga hotspots likely are incorporated into the Lau Basin via direct subduction, Samoan islands and seamounts lie too far north of the Tonga Trench to subduct (Figure 1). Therefore, it is thought that a present-day Samoan plume component is entrained in a toroidal mantle flow field generated by the subducting Tonga slab as it undergoes slab roll back (Figure 9) [e.g., *Turner and Hawkesworth*, 1998; *Druken et al*., 2014; *Price et al*., 2014]. The incorporation of nearby Samoan plume material into the Lau Basin has long been used to explain the unusually high $^{3}He/^{4}He$ (up to 28.1 Ra) [*Lupton et al*., 2009] found in some Lau Basin lavas [e.g., *Poreda and Craig*, 1992; *Hilton et al*., 1993; *Honda et al*., 1993; *Lupton et al*., 2009; *Hahm et al*., 2012; *Lupton et al*., 2012a, 2012b] and subsequent isotopic studies of Lau Basin lavas have shown that moderately enriched Lau Basin lavas have Hf-Pb-Sr-Nd isotopic values consistent with a mixture of incorporated Samoan plume material and ambient mantle [*Volpe et al*., 1988; *Poreda and Craig*, 1992; *Danyushevsky et al*., 1995; *Regelous et al*., 2008; *Tian et al*., 2008; *Escrig et al*., 2009; *Tian et al*., 2011; *Escrig et al*., 2012; *Lytle et al*., 2012; *Price et al*., 2014]. Below, we discuss the isotopic evidence, which shows that Samoan components are present in a subset of the new lavas from the NELB.

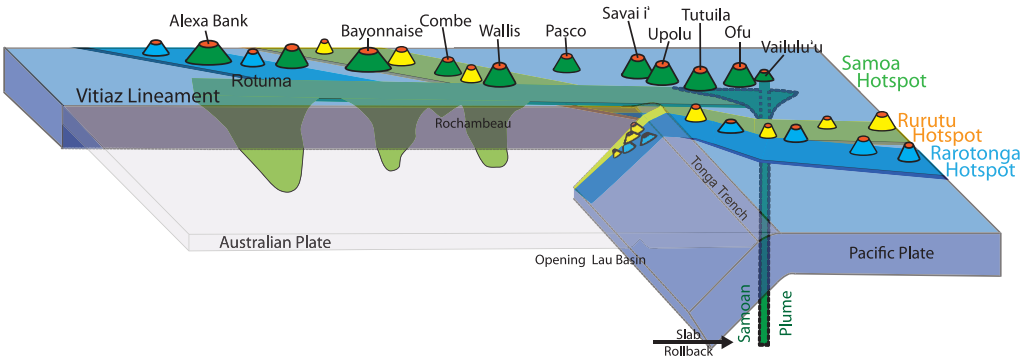

Figure 9. Cartoon schematic showing the Lau Basin and the seamount trail traces of the Rurutu, Rarotonga, and Samoa hotspots. Seamounts defining the older portions of the Rarotonga and Rurutu hotspots are predicted to subduct into the northernmost region of the Tonga trench, beneath the NELB, imprinting their geochemical signatures, HIMU and EM1, respectively, on the mantle wedge of the NELB. These signatures are then expressed in back-arc basin lavas from the NELB. Incorporation of Samoan plume material into NELB, caused by toroidal flow around the Tonga slab, is widespread in the northern Lau and North Fiji Basins [*Price* et al. 2014].

4.2. Origin of Isotopic Diversity in the New NELB Lavas

Along with the reconstructed hotspot tracks (which intersect the Tonga trench near the NELB) discussed above, spatial variations in Hf, Pb, Sr, Nd, and He isotopic compositions in the NELB can be used to identify the different components sampled by the lavas of this study. Here we model the geochemical variability in the Lau Basin using presubducted protolith compositions (i.e., we use the trace element and isotopic compositions from seamounts and islands from the Cook-Austral volcanic chain) and mix these components in the mantle wedge to generate sources for the lavas in the northern Lau Basin. This is an approach that has been adopted previously [i.e., *Turner and Hawkesworth*, 1998; *Falloon et al*., 2007] to model the mantle sources of lavas in the Lau Basin and Tonga arc. A potential drawback to this modeling approach is that trace element abundances and ratios of the presubducted protoliths may be modified during subduction zone processing as the relevant trace elements likely exhibit differential fluid mobility in the slab during subduction, where Pb is more fluid mobile than Sr, which in turn is more mobile than Nd and Hf [*Kessel et al*., 2005] (see section 4.3 below). While we acknowledge this is an uncertainty in our mixing models, we note that the mixing models do a reasonably good job at describing the geochemical variability seen in the new NELB lavas. This may be because, at the highest temperatures and pressures, relative fluid mobilities of Hf, Pb, Sr, and Nd become more similar [*Kessel et al*., 2005].

The first geochemically distinct group of lavas from dredge D44, D44-HIMU, has the most radiogenic Pb isotopic ratios identified in the Lau Basin to date. While these lavas do not host end-member HIMU signatures, they have a larger contribution from a HIMU source than any lava previously characterized from the Lau Basin. In most isotopic spaces, lavas from the D44-HIMU group consistently plot in, or near, the field defined by Rurutu hotspot lavas (Figures 5 and 6). However, D44-HIMU lavas are geochemically enriched compared to the end-member HIMU Rurutu hotspot lavas and, in a plot of $^{143}Nd/^{144}Nd$ versus $^{87}Sr/^{86}Sr$ (Figure 5), are shifted toward an EM1 component similar to Uo Mamae. In all isotopic spaces, the D44-HIMU lavas plot between the fields for Uo Mamae lavas and HIMU lavas from the Rurutu hotspot. We present a mixing model that generates compositions (in multiple isotopic spaces) that are similar to the D44-HIMU lavas when a Rurutu hotspot lava component is mixed with an Uo Mamae lava component (see Figures 5 and 6 for the D44-HIMU modeled mixing lines and Table 5 for mixing parameters). Unfortunately, relatively little Hf isotopic data exist for the Cook-Austral islands and seamounts. Therefore, the mixing model (and subsequent mixing models for the other lavas in this study) is not evaluated in $^{176}Hf/^{177}Hf$–$^{143}Nd/^{144}Nd$ space. A more detailed description of this mixing model (and the mixing models discussed below) is provided in the supporting information.

The second geochemical group of lavas from dredge D44, designated D44-EM, consists of boninite series lavas that have the highest $^{87}Sr/^{86}Sr$ in this study. The D44-EM lavas still have relatively high $^{207}Pb/^{204}Pb$ (up to 15.642), although not as high as the D44-HIMU lavas (Figure 5), and are shifted toward a component with relatively high $^{206}Pb/^{204}Pb$ and $^{208}Pb/^{204}Pb$ (such as the Rurutu hotspot) in all isotopic spaces. In plots showing Sr and Nd isotopic ratios versus $^{207}Pb/^{204}Pb$, the D44-EM lavas fall in the field defined by lavas from the

AGU Geochemistry, Geophysics, Geosystems

10.1002/2015GC006237

Table 5. Parameters for Mixing Models shown in Figures 5 and 6

	Sr (ppm)	Nd (ppm)	Pb (ppm)	$^{87}Sr/^{86}Sr$	$^{143}Nd/^{144}Nd$	$^{206}Pb/^{204}Pb$	$^{207}Pb/^{204}Pb$	$^{208}Pb/^{204}Pb$
Mixing model 1 (Mixing model for generating D44-HIMU lavas)[a]:								
Mixing endmember 1: Uo Mamae seamount	705.0	40.0	4.9	0.705215	0.512470	18.3317	15.6372	38.5210
Data sources	*Falloon et al.* [2007] Sample 16-94/1	*Falloon et al.* [2007] Sample 16-94/1	*Falloon et al.* [2007] Sample 16-94/1	*Falloon et al.* [2007] Sample 16-94/1	*Falloon et al.* [2007] Sample 16-94/1	*Falloon et al.* [2007] Sample 16-94/1	*Falloon et al.* [2007] Sample 16-94/1	*Falloon et al.* [2007] Sample 16-94/1
Mixing endmember 2: Rurutu hotspot	663.0	70.0	4.6	0.702992	0.512915	20.3960	15.6830	39.9655
Data sources	*Nakamura and Tatsumoto* [1988]; Sample MK-73	*Nakamura and Tatsumoto* [1988]; Sample MK-73	*Nakamura and Tatsumoto* [1988]; Sample MK-73	*Bonneville et al.* [2006]; Average of samples DR07 (Arago) and DR02-1 (ZEP2-12)	*Bonneville et al.* [2006]; Average of samples DR07 (Arago) and DR02-1 (ZEP2-12)	*Bonneville et al.* [2006]; Average of samples DR07 (Arago) and DR02-1 (ZEP2-12)	*Bonneville et al.* [2006]; Average of samples DR07 (Arago) and DR02-1 (ZEP2-12)	*Bonneville et al.* [2006]; Average of samples DR07 (Arago) and DR02-1 (ZEP2-12)
Mixing model 2 (Mixing model for generating D44-EM lavas)[b]:								
Mixing endmember 1: Upolu and Savai'i Island rejuvenated series	794.5	37.3	3.8	0.705510	0.512622	18.5720	15.6050	38.7590
Data sources	*Workman et al.* [2004]; Sample S 52 M	*Workman et al.* [2004]; Sample S 52 M	*Workman et al.* [2004]; Sample S 52 M	*Wright and White* [1987]; Sample 82UP-43	*Wright and White* [1987]; Sample 82UP-43	*Wright and White* [1987]; Sample 82UP-43	*Wright and White* [1987]; Sample 82UP-43	*Wright and White* [1987]; Sample 82UP-43
Mixing endmember 2: Rurutu hotspot	943.0	61.4	2.6	0.703388	0.512915	20.3500	15.6900	39.8200
Data sources	*Chauvel et al.* [1997]; Average of Samples RR30 RR59 and RRT-15	*Chauvel et al.* [1997]; Average of Samples RR30 RR59 and RRT-15	*Chauvel et al.* [1997]; Average of Samples RR30 RR59 and RRT-15	*Chauvel et al.* [1997]; Average of Samples RR30 RR59 and RRT-15	*Chauvel et al.* [1997]; Average of Samples RR30 RR59 and RRT-15	*Chauvel et al.* [1997]; Average of Samples RR30 RR59 and RRT-15	*Chauvel et al.* [1997]; Average of Samples RR30 RR59 and RRT-15	*Chauvel et al.* [1997]; Average of Samples RR30 RR59 and RRT-15
Mixing model 3 (Mixing model for generating D44-depleted lava)[c]:								
Mixing endmember 1: Depleted Lau Basin Mantle component (Eastern Lau Spreading Center)	95.0	4.4	0.5	0.703191	0.513100	18.0800	15.5250	37.9830
Data sources	*Escrig et al.* [2009]; ELSC sample RC098	*Escrig et al.* [2009]; ELSC sample RC098	*Escrig et al.* [2009]; ELSC sample RC098	*Hergt and Woodhead* [2007]; ELSC sample 24.1.1	*Hergt and Woodhead* [2007]; ELSC sample 24.1.1	*Hergt and Woodhead* [2007]; ELSC sample 24.1.1	*Hergt and Woodhead* [2007]; ELSC sample 24.1.1	*Hergt and Woodhead* [2007]; ELSC sample 24.1.1
Mixing endmember 2: Ofu Island Shield series	1058.0	93.0	6.1	0.705215	0.512738	19.4178	15.6259	39.7801
Data sources	*Hart and Jackson* [2014]; Ofu sample Ofu-04-07	*Hart and Jackson* [2014]; Ofu sample Ofu-04-07	*Hart and Jackson* [2014]; Ofu sample Ofu-04-07	*Hart and Jackson* [2014]; Ofu sample Ofu-04-07	*Hart and Jackson* [2014]; Ofu sample Ofu-04-07	*Hart and Jackson* [2014]; Ofu sample Ofu-04-07	*Hart and Jackson* [2014]; Ofu sample Ofu-04-07	*Hart and Jackson* [2014]; Ofu sample Ofu-04-07

Geochemistry, Geophysics, Geosystems

10.1002/2015GC006237

Table 5. (continued)

	Sr (ppm)	Nd (ppm)	Pb (ppm)	$^{87}Sr/^{86}Sr$	$^{143}Nd/^{144}Nd$	$^{206}Pb/^{204}Pb$	$^{207}Pb/^{204}Pb$	$^{208}Pb/^{204}Pb$
Mixing model 4 (Mixing model for generating D42 lavas)[d]:								
Mixing endmember 1: Uo Mamae Island	959.0	79.4	8.2	0.705222	0.512511	18.4270	15.6310	38.6040
Data sources	*Pearce et al.* [2007]; Sample 16-95-2	*Pearce et al.* [2007]; Sample 16-95-2	*Pearce et al.* [2007]; Sample 16-95-2	*Pearce et al.* [2007]; Sample 16-95-2	*Pearce et al.* [2007]; Sample 16-95-2	*Pearce et al.* [2007]; Sample 16-95-2	*Pearce et al.* [2007]; Sample 16-95-2	*Pearce et al.* [2007]; Sample 16-95-2
Mixing endmember 2: Rurutu hotspot	367.0	42.3	2.2	0.702613	0.512912	20.3330	15.6580	39.9530
Data sources	*Nakamura and Tatsumoto* [1988]; Sample AT83_A	*Nakamura and Tatsumoto* [1988]; Sample AT83_A	*Nakamura and Tatsumoto* [1988]; Sample AT83_A	*Bonneville et al.* [2006]; Sample ZEP2-12	*Bonneville et al.* [2006]; Sample ZEP2-12	*Bonneville et al.* [2006]; Sample ZEP2-12	*Bonneville et al.* [2006]; Sample ZEP2-12	*Bonneville et al.* [2006]; Sample ZEP2-12

[a]Notes on mixing model 1: We use isotopic and trace element data from a single lava, sample 16-94/1, from Uo Mamae seamount (which has a strong EM1 signature) as one end-member for our mixing model. The second end-member uses isotopic data taken from the average of two lavas from two Rurutu seamounts, Arago and ZEP2-12. Trace element data for these lavas are not available, so we use trace element data from another Rurutu hotspot island (Mauke), which provides the best trace element match for the mixing model.

[b]Notes on mixing model 2: Isotopic data from the Samoa rejuvenated lava used as an end-member in the mixing model comes from a single rejuvenated lava from Upolu Island. Since no trace element data exist for this sample, we use trace element concentrations taken from a Savai'i rejuvenated lava to constrain the Samoan rejuvenated end-member. The Rurutu end-member of the mixing model is defined by isotopic data from an average of three Rurutu lavas (samples RRT-15, RR30, and RR59, all from the younger series of volcanism on the island) and trace element data from the average of samples RRT-15 and RR59 (trace element data for sample RR30 do not exist).

[c]Notes on mixing model 3: The Samoan shield end-member isotope compositions and trace element concentrations are taken from a single lava from Ofu island; while He isotopic data are not available for this sample, all Ofu island lavas with measured He isotopic compositions have elevated ratios that vary form 19.5 to 33.8 Ra. A single lava sample from the Eastern Lau Spreading Center (ELSC), sample 41.1.1 from Hergt and Woodhead (2007), provides a suitable isotopic composition for the depleted mantle end-member in the Lau Basin. However, this sample has no reported trace element data, hence trace element data from another ELSC lava, sample RC098, from Escrig et al. (2009) is used in the model.

[d]Notes on mixing model 4: We use isotopic data and trace element concentrations from a single Uo Mamae Island lava (sample 16/95-2) as the first end-member for the dredge 42 mixing model. We use isotopic data from a single Rurutu lava from seamount ZEP2-12 to represent the Rurutu end-member. Trace element data for this seamount are not available so we instead use values from another Rurutu hotspot island, Aitu, for the Rurutu end-member of the mixing model.

Rurutu hotspot (Figure 6). However, like D44-HIMU lavas, in multiple isotopic spaces (e.g., $^{206}Pb/^{204}Pb$ versus $^{87}Sr/^{86}Sr$), D44-EM samples are shifted away from the field of Rurutu hotspot lavas toward a second component with an enriched mantle composition with higher $^{87}Sr/^{86}Sr$, lower $^{143}Nd/^{144}Nd$, and lower $^{206}Pb/^{204}Pb$. This component is similar to rejuvenated lavas found in Samoa. We find that a mixture of the Samoan hotspot component and a subducted HIMU component (from subducted seamounts and volcanoclastic material with compositions similar to that identified in the Rurutu hotspot) is required to match the composition of D44-EM lavas (see Figures 5 and 6 for D44-EM modeled mixing lines and Table 5 for mixing parameters for D44-EM lavas).

The third and final geochemical group from dredge D44, D44-depleted, is defined by a single lava that shows the least radiogenic $^{87}Sr/^{86}Sr$ (0.704008) and Pb isotopic signatures ($^{206}Pb/^{204}Pb$ of 18.637, $^{207}Pb/^{204}Pb$ of 15.570, and $^{208}Pb/^{204}Pb$ of 39.095), and the most radiogenic $^{143}Nd/^{144}Nd$ (0.512889) and $^{176}Hf/^{177}Hf$ (0.283109) of the lavas reported in this study. The D44-depleted sample is the only lava from the present sample suite with high $^{3}He/^{4}He$ (19.3 Ra), a signature that has been observed previously in the Lau Basin and is attributed to the incorporation of a high $^{3}He/^{4}He$ Samoan plume component in the Lau Basin [e.g., *Poreda and Craig*, 1992; *Hilton et al*., 1993; *Honda et al*., 1993; *Lupton et al*., 2009; *Hahm et al*., 2012; *Lupton et al*., 2012a, 2012b]. The isotopic compositions of this lava are relatively well matched by mixing a geochemically depleted melt from the Lau Basin (similar in composition to depleted lavas from the ELSC) [*Escrig et al*., 2009; *Hergt and Woodhead*, 2007] with a shield component similar to the Samoan island of Ofu, the island with the highest $^{3}He/^{4}He$ (33.8 Ra) from the Samoan hotspot [*Jackson et al*., 2007b, 2009; *Hart and Jackson*, 2014] (see Table 5 for mixing parameters and Figures 5 and 6 for modeled mixing lines for the D44-depleted lava).

Dredge D42 lavas also exhibit relatively radiogenic Pb isotopic compositions compared to other Lau Basin lavas, and a Rurutu hotspot component is also needed to generate the HIMU signatures in these lavas (Figure 6). The dredge D42 samples are shifted away from the field of Rurutu hotspot lavas toward a component with an enriched mantle (EM) composition that, in this case, is similar to that of Uo Mamae. Our mixing model, which includes Rurutu hotspot and Uo Mamae components, consistently reproduces compositions that are similar to the new isotopic data for dredge D42 lavas (see Table 5 and Figures 5 and 6 for the D42 mixing parameters and modeled mixing lines, respectively).

4.3. Trace Element Signatures From Arc Processes

The radiogenic isotopic compositions of the Lau Basin lavas presented here are relatively enriched geochemically and are interpreted to result from the incorporation of various hotspot signatures into their source domains. However, the trace element signatures, including Ba/Nb and Ce/Pb ratios, are quite different from the ocean island basalt lavas erupted at the hotspots suggested to be contributing to the Lau Basin. Rather, most of the NELB lavas presented here exhibit arc-like trace element signatures, including high Ba/Nb and low Ce/Pb ratios (Figure 4). We argue that these trace element signatures differ from those in hotspot lavas (from Rurutu and Rarotonga hotspots) because the Rurutu and Rarotonga hotspot components sampled in the NELB result from subduction (and subduction zone processing).

Geochemical signatures from the Tonga subduction zone, including components of slab or sediment-derived melts and fluids, are found in Tonga arc lavas, but also in a spatially limited subset of Lau back-arc basin lavas [e.g., *Regelous et al*., 1997; *Turner et al*., 1997; *Ewart et al*., 1998; *Peate et al*., 2001; *Hergt and Woodhead*, 2007; *Escrig et al*., 2009]. Barium and Nb, as well as Ce and Pb, are strongly fractionated in subduction zones; lavas from the Tonga arc are characterized by elevated Ba/Nb and low Ce/Pb ratios (Figures 10a and 10b). Lau Basin back-arc lavas with high Ba/Nb, such as lavas from the Fonualei Spreading Center (FRSC) and ELSC [e.g., *Escrig et al*., 2009, 2012], are thought to have incorporated an arc component. Lavas from the FRSC and ELSC overlap Tonga arc lavas in a plot of Ba/Nb versus $^{143}Nd/^{144}Nd$ (Figure 10a). Similarly, FRSC and ELSC lavas have low Ce/Pb and overlap Tonga arc lavas in a plot of Ce/Pb versus $^{208}Pb/^{204}Pb$, supporting the incorporation of slab-derived materials. Ba/Nb and Ce/Pb ratios in other Lau Basin lavas (e.g., Mangatolu Triple Junction) suggest less extreme contributions from the arc (Figure 10). Thus, Ba/Nb and Ce/Pb can be used as indicators of the presence of an arc component in Lau Basin lavas.

Lavas previously examined from the NELB have elevated Ba/Nb and low Ce/Pb [*Falloon et al*., 2007] and like lavas from the FRSC and ELSC, they trend toward and overlap Tonga arc lavas in Figure 10. Dredge D42, D44-HIMU, and D44-EM lavas in the NELB also exhibit high Ba/Nb and low Ce/Pb that suggest an arc

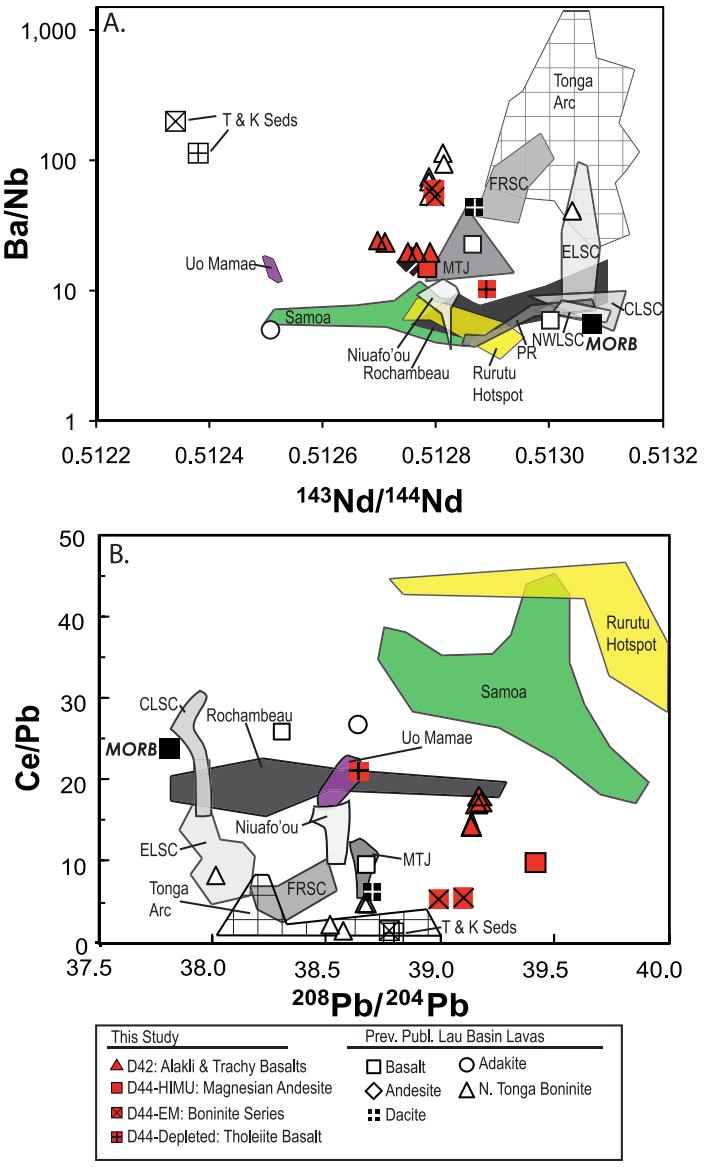

Figure 10. (a) Ba/Nb versus $^{143}Nd/^{144}Nd$, while (b) shows Ce/Pb versus $^{208}Pb/^{204}Pb$ for new and previously published data from the region. Some of the new samples appear to be influenced by the arc, but not by the addition of Tonga or Kermadec sediment. Samoan field includes lavas only from Upolu, Tau, and Malumalu Islands after *Regelous et al.* [2008]. Samoan data are from *Wright and White* [1987], *Poreda and Craig* [1992], *Workman et al.* [2004], *Workman and Hart* [2005], *Jackson et al.* [2007a, 2007b, 2010], and *Hart and Jackson* [2014]. Previously published data from the NELB are taken from *Falloon and Crawford* [1991]; *Danyushevsky et al.* [1995]; *Falloon et al.* [2007, 2008] and symbols are the same as Figure 5. Values for MORB are taken from *Gale et al.* [2013]. The Tonga and Kermadec bulk sediment data are from *Plank and Langmuir* [1998]. Tonga Arc data are from *Ewart et al.* [1998], *Hergt and Woodhead* [2007], *Pearce et al.* [2007], *Escrig et al.* [2012], *Turner et al.* [2012], and *Caulfield et al.* [2015]. Fonualei Rift and Spreading center data are from *Escrig et al.* [2012]. The ELSC data are from *Escrig et al.* [2009], while the CLSC data are from *Volpe et al.* [1988], *Pearce et al.* [1994], *Hergt and Woodhead* [2007], and *Tian et al.* [2008]. NWLSC data are from *Jenner et al.* [2012] and *Lytle et al.* [2012]. Peggy Ridge data are from *Volpe et al.* [1988], *Tian et al.* [2011], and *Price et al.* [2014]. Niuafo'ou data are from *Volpe et al.* [1988], *Regelous et al.* [2008], and *Tian et al.* [2011], while Mangatolu Triple Junction data are from *Volpe et al.* [1988], *Falloon et al.* [1992], and *Tian et al.* [2011]. Rochambeau Bank and Rift data are from *Poreda and Craig* [1992], *Lytle et al.* [2012], and *Tian et al.* [2011]. Rurutu hotspot data are from Rurutu Hotspot islands and are taken from *Dupuy et al.* [1989], *Chauvel et al.* [1997], *Salters et al.* [2011] and *Hanyu et al.* [2011]. Uo Mamae data are from *Falloon et al.* [2007], *Pearce et al.* [2007], and *Regelous et al.* [2008].

signature (Figure 10). For example, the magnesian andesite whole rock D44-26 (a D44-HIMU type lava) has elevated Ba/Nb (14.9) and low Ce/Pb (9.9) compared to average global MORB (with values of 5.6 and 26.1, respectively) [*Gale et al.*, 2013]. The D44-EM boninite series lavas have even higher Ba/Nb signatures (ranging from 52.2 to 60.5) similar to the highest values observed in the Lau Basin, and have the lowest Ce/Pb ratios (ranging from 5.4 to 5.8) of this study (Figure 10b.) The dredge D42 lavas have a range of Ba/Nb (19.5 to 24.1) and Ce/Pb (14.4 to 18.0) ratios that also suggest the presence of an arc component. In contrast to the other lavas in this study, the D44-depleted lava (sample D44-91) does not show clear evidence from trace element systematics for an arc component (Ba/Nb = 10.2; Ce/Pb = 21.1). Instead, this high-$^{3}He/^{4}He$ lava is characterized by geochemically depleted trace element and isotopic signatures. The absence of a clear arc component in this lava may be because neither of the components thought to comprise the source of this lava—a depleted Lau Basin component and a high $^{3}He/^{4}He$ Samoan component—require processing in the Tonga arc (section 4.2).

Dredge D42, D44-HIMU, and D44-EM lavas host components that appear to have been processed in the Tonga arc, including subducted seamounts from the Rarotonga and Rurutu hotspots that contributed EM1 and HIMU components, as these lavas have radiogenic isotopic signatures that overlap with the range of values identified in the Rarotonga (Uo Mamae) and Rurutu hotspots. An important question is whether the

components in the mantle source of the D44-EM lavas reveal the mechanism responsible for their boninite petrogenesis. The D44-EM lavas sample subducted Rurutu hotspot seamounts as well as a component from the Samoan mantle, and the combination of these components may provide clues about the petrogenesis of these boninite-series lavas, which require a unique combination of high temperatures at shallow depth, fluids, and a refractory mantle wedge [e.g., *Crawford et al*., 1989; *Sobolev and Danyushevsky*, 1994; *Danyushevsky et al*., 1995; *Resing et al*., 2011]: It has been suggested that Tongan boninites require temperatures as high as ~1480°C at depths of ~45 km in the mantle wedge [*Sobolev and Danyushevsky*, 1994; *Falloon and Danyushevsky*, 2000]. Incorporation of hot, refractory Samoan plume mantle to the region could provide the heat needed at shallow depth for boninite petrogenesis [e.g., *Danyushevsky et al*., 1995; *Falloon et al*., 2007, 2008; *Resing et al*., 2011]. Additionally, the subducted Rurutu hotspot seamounts (which contribute to the mantle source of the D44-EM lavas) would dehydrate during subduction, thereby providing the fluids needed to flux the hot refractory Samoan mantle component and aid boninite petrogenesis. Notably, the boninitic D44-EM lavas are the only lavas in this study that have both a Samoan component and a subducted hotspot component: The other lavas in this study with subducted seamount signatures (D44-HIMU and dredge D42 lavas) are not boninitic in composition, and this may relate to the fact that they lack a Samoan component (and therefore the heat provided by the Samoan plume) required for boninite petrogenesis. Finally, the D44-depleted lava does host a Samoan component, but it is not boninitic. This may be because this lava does not sample a subducted component, which may be required to provide fluids for fluxing the mantle during boninite petrogenesis. In summary, the petrogenesis of northern Tonga boninites may require *both* a subducted crust component (to provide fluids) and a Samoan component (to provide heat).

4.4. Extent and Origin of the Various Plume Signatures in the NELB

Unlike Samoan geochemical signatures, which are found over broad areas in the Lau Basin [e.g., *Volpe et al*., 1988; *Poreda and Craig*, 1992; *Wendt et al*., 1997; *Tian et al*., 2008; *Lupton et al*., 2009; *Tian et al*., 2011; *Hahm et al*., 2012; *Lupton et al*., 2012b, 2012b; *Lytle et al*., 2012; *Price et al*., 2014; *Nebel and Arculus*, 2015], the HIMU and EM1 signatures are absent from lavas outside of the NELB (Figure 8b). The map in Figure 8b shows that the lavas with the most extreme HIMU and EM1 signatures—highest $^{207}Pb/^{204}Pb$ and lowest $^{143}Nd/^{144}Nd$, indicative of inputs from the Rurutu and Rarotonga hotspots, respectively—in the Lau Basin are from the NELB and are not found elsewhere in the region. The new lavas not only show pronounced HIMU and EM1 signatures in the region, but also lie in the region of the Lau Basin closest to where the reconstructed hotspot tracks of Rurutu (a HIMU hotspot) and Rarotonga (an EM1 hotspot) intersect the Tonga Trench (Figure 1). The geographic correspondence of the enriched Lau Basin lavas (including EM1 and HIMU components) with the location of subduction of the Rarotonga and Rurutu hotspots in the northern Tonga arc is striking and provides a powerful argument in favor of a model where two of the three Cook-Austral hotspots are contributing subducted seamount components to the northern-most parts of the Lau Basin.

While it has previously been suggested that the isotopically enriched mantle sources in the northern portions of the Lau Basin are due to the incursion of enriched Indian-type mantle material from the north [e.g., *Pearce et al*., 2007], we argue for a different origin of the enriched geochemical signatures in the NELB. We suggest that the EM1 and HIMU geochemical signatures observed in the NELB result from the inflow of Samoan plume material and subduction of seamounts (and their volcaniclastic aprons) belonging to the Cook-Austral hotspots. The Cook-Austral-like geochemical signatures seen in the NELB lavas have their origin in hotspot volcanism generated over deeply sourced mantle plumes [*Konter et al*., 2008] that feed the Rurutu and Rarotonga hotspots (Figure 9). The geochemically enriched isotopic signatures associated with hotspot volcanoes in the South Pacific have been referred to as a DUPAL signature, a globe-encircling feature of mantle enrichment identified primarily in hotspots erupted in the southern hemisphere [*Hart*, 1984]. Both the Rurutu and Rarotonga hotspots are suggested to be long-lived (up to 100 Ma or older) and thus may be the oldest hotspots in the Pacific [*Koppers et al*., 2003; *Konter et al*., 2008]. Both hotspots are anchored over the Pacific large low-shear-velocity province (LLSVP) [*Torsvik et al*., 2010; *McNamara et al*., 2010; *Mukhopadhyay*, 2012; *Li et al*., 2014], which is one of two (the other is located in the deep mantle beneath Africa) antipodal regions of anomalously low seismic shear velocity identified in the deepest mantle above the core-mantle boundary. Ocean island basalts with the strongest DUPAL anomalies have been suggested to overlie both LLSVPs [*Castillo*, 1988]. This provides a strong argument that DUPAL signatures observed in basalts erupted at Earth's surface trace their origins

to the deepest mantle LLSVPs and require buoyantly upwelling mantle plumes to transport this material to shallow asthenospheric depths, where it generates melt and produces, for example, the Rurutu and Rarotonga hotspot volcanism. After formation of the HIMU and EM1 volcanoes over each of these two Cook-Austral hotspots, the seamounts are rafted toward the Tonga Trench (as the Pacific plate moves westward) and subducted beneath the Lau Basin. The geochemically distinctive EM1 and HIMU isotopic signatures associated with these seamounts are then imparted to the lavas of the NELB as they undergo dehydration metamorphic reactions during subduction. As a result, we suggest that the NELB lavas exhibit isotopic signatures ultimately derived from the deepest mantle, as well as trace element patterns that reflect arc-like signatures acquired during seamount subduction of the older portions of DUPAL hotspots in the Lau Basin (Figure 9).

5. Conclusions

We analyzed 11 samples from two new dredge locations in the northeast Lau Basin in order to investigate potential sources of enriched and HIMU mantle material in the region. Using reconstructions of hotspot tracks emerging from the Cook-Austral volcanic lineament, we find it unlikely that seamounts related to the HIMU Macdonald hotspot have subducted under the Lau Basin. However, the reconstructed hotspot tracks from the Rurutu (HIMU) and Rarotonga (EM1) hotspots show that older volcanoes associated with these hotspots likely subducted into the Tonga Trench. During subduction, these volcanoes and seamounts imparted their HIMU and EM1 signatures to the NELB mantle. We further demonstrate that the new NELB lavas presented in this study, which range from 1.3 Ma to 0.365 Ma in age, show geochemically enriched $^{143}Nd/^{144}Nd$ (values down to 0.512697 in dredge D42) and the most radiogenic Pb isotopic ratios (values up to 19.580 in dredge D44) to date in the Lau Basin. These signatures are best explained by the incorporation of HIMU and EM1 geochemical signatures into the mantle sources of these lavas. These HIMU and EMI signatures are likely associated with the Rurutu and Rarotonga hotspots, respectively, as the reconstructed traces of these two hotpots intersect the northernmost Tonga trench near the region of the NELB where the samples from this study were recovered. A subset of lavas from dredge D44 also exhibit evidence for the sampling of mantle sources that host a Samoan component in addition to the subducted components (HIMU and EM1) from the Cook-Austral volcanic lineament, and one of these subsets constitute the westernmost observation of boninites in the Lau Basin. Finally, one new lava from the NELB presented here (D44-91) has $^{3}He/^{4}He$ of 19.3 Ra. This lava was recovered to the northeast of lavas previously discovered to have high $^{3}He/^{4}He$ (e.g., Rochambeau Bank and Rifts) and broadens the eastern and northern extent of a high $^{3}He/^{4}He$ (Samoan) signature, and hence, the region of Samoan influence, in the Lau Basin.

Acknowledgements

We acknowledge helpful reviews from Bill White and Marcel Regelous. Efficient editorial handling by Thorsten Becker is appreciated. We thank Paterno *Castillo* and James Natland for discussions, and Joshua Curtice for assistance with the helium measurements. We are grateful to the scientific party and the ship's crew of the R/V Roger Revelle on the RR1310 cruise to the Tuvalu islands. MGJ acknowledges support from NSF grants OCE-1153894, EAR-1347377, EAR-1145202, and EAR-1348082. J.B.T. acknowledges support from the French Agence Nationale de la Recherche grant ANR-10-BLANC-0603 M&Ms – Mantle Melting – Measurements, Models, Mechanisms. A.A.P.K. and C.S.C. acknowledge support from NSF grant OCE-1154070, M.D.K. from NSF grant OCE-1232985, and J.G.K. from NSF grants OCE-1153959 and OCE-1433097.

References

Abouchami, W., S. J. G. Galer, and A. W. Hofmann (2000), High precision lead isotope systematics of lavas from the Hawaiian Scientific Drilling Project, *Chem. Geol.*, *169*(1), 187–209.

Becker, J. J., et al. (2009) Global bathymetry and elevation data at 30 arc seconds resolution: SRTM30_PLUS, *Mar. Geod.*, *32*, 355–371, doi: 10.1080/01490410903297766.

Beier, C., L. Vanderkluysen, M. Regelous, J. J. Mahoney, and D. Garbe-Schönberg (2011) Lithospheric control on geochemical composition along the Louisville Seamount Chain, *Geochem. Geophys. Geosyst.*, *12*, Q0AM01, doi:10.1029/2011GC003690.

Blichert-Toft, J. (2001), On the Lu-Hf Isotope geochemistry of silicate rocks, *Geostand. Newsl.*, *25*(1), 41–56.

Blichert-Toft, J., and F. Albarède (1997), The Lu-Hf isotope geochemistry of chondrites and the evolution of the mantle-crust system, *Earth Planet. Sci. Lett.*, *148*(1), 243–258.

Blichert-Toft, J., C. Chauvel, and F. Albarede (1997), Separation of Hf and Lu for high-precision isotope analysis of rock samples by magnetic sector-multiple collector ICP-MS, *Contrib. Mineral. Petrol.*, *127*(3), 248–260.

Bonneville, A., R. Le Suavé, L. Audin, V. Clouard, L. Dosso, P. Y. Gillot, P. Janney, K. Jordahl, and K. Maamaatuaiahutapu (2002), Arago Seamount: The missing hotspot found in the Austral Islands, *Geology*, *30*(11), 1023–1026.

Bonneville, A., L. Dosso, and A. Hildenbrand (2006), Temporal evolution and geochemical variability of the South Pacific superplume activity, *Earth Planet. Sci. Lett.*, *244*, 251–269, doi:10.1016/j.epsl.2005.12.037.

Castillo, P. R. (1988), The Dupal anomaly as a trace of upwelling lower mantle, *Nature*, *336*, 667–670.

Castillo, P. R. (2012), Adakite petrogenesis, *Lithos*, *134*, 304–316.

Castillo, P. R., P. F. Lonsdale, C. L. Moran, and J. W. Hawkins (2009), Geochemistry of mid-Cretaceous Pacific crust being subducted along the Tonga–Kermadec Trench: Implications for the generation of arc lavas, *Lithos*, *112*(1), 87–102.

Caulfield, J., S. Turner, R. Arculus, C. Dale, F. Jenner, J. Pearce, C. Macpherson, and H. Handley (2012), Mantle flow, volatiles, slab-surface temperatures and melting dynamics in the north Tonga arc–Lau back-arc basin, *J. Geophys. Res.*, *117*, B11209, doi:10.1029/2012JB009526.

Caulfield, J., J. Blichert-Toft, F. Albarede, and S. Turner (2015), Corrigendum to "Magma evolution in the primitive, intra-oceanic Tonga arc: Petrogenesis of Basaltic Andesites at Tofua Volcano" and 'Magma evolution in the Primitive, Intra-oceanic Tonga arc: Rapid Petrogenesis of Dacites at Fonualei Volcano', *J. Petrol.*, *56*(3), 641–644.
Chauvel, C., A. W. Hofmann, and P. Vidal (1992), HIMU–EM: The French Polynesian connection, *Earth Planet. Sci. Lett.*, *110*(1), 99–119.
Chauvel, C, W. F. McDonough, G. Guille, R. Maury, and R. Duncan (1997), Contrasting old and young volcanism in Rurutu Island, Austral chain, *Chem. Geol.*, *139*(1), 125–143.
Cheng, Q., K. Park, J. D. Macdougall, A. Zindler, G. W. Lugmair, H. Staudigel, J. Hawkins, and P. Lonsdale (1987), Isotopic evidence for a hotspot origin of the Louisville seamount chain, *Geophys. Monogr.-Seamounts, Islands, and Atolls*, *43*, 1–14.
Clague, D. A., and D. R. Sherrod (2014), Growth and degradation of Hawaiian volcanoes: Chapter 3 in Characteristics of Hawaiian volcanoes, *U.S. Geol. Surv. Prof. Pap., 1801-3*, pp. 97–146.
Cooper, L. B., T. Plank, R. J. Arculus, E. H. Hauri, P. S. Hall, and S. W. Parman (2010), High-Ca boninites from the active Tonga Arc, *J. Geophys. Res.*, *115*, B10206, doi:10.1029/2009JB006367.
Crawford, A. J., T. J. Falloon, and D. H. Green (1989), Classification, petrogenesis and tectonic setting of boninites, Boninites, edited by A. J. Crawford, pp. 1–49, Unwin Hyman, London, U. K.
Danyushevsky, L. V., A. V. Sobolev, and T. J. Falloon (1995), North Tongan high-Ca boninite petrogenesis: The role of Samoan plume and subduction zone-transform fault transition, *J. Geodyn.*, *20*(3), 219–241.
Diraison, C. (1991), *Le volcanisme aérien des archipels polynésiens de la Société, des Marquises et des Australes-Cook. Téphrostratigraphie, datation isotopique et géochimie comparées. Contribution à l'étude des origines du volcanisme intraplaque du Pacifique Central* – Thèse de Doctorat, Univ. Bretagne Occiden- tale, Brest, 413 pp., dissertation.
Druken, K. A., C. Kincaid, R. W. Griffiths, D. R. Stegman, and S. R. Hart (2014), Plume–slab interaction: The Samoa–Tonga system, *Phys. Earth Planet. Inter.*, *232*, 1–14.
Duncan, R. A., and I. McDougall (1976), Linear volcanism in French polynesia, *J. Volcanol. Geotherm. Res.*, *1*(3), 197–227.
Dupuy, C., H. G. Barsczus, J. Dostal, P. Vidal, and J. M. Liotard (1989), Subducted and recycled lithosphere as the mantle source of ocean island basalts from southern Polynesia, central Pacific, *Chem. Geol.*, *77*(1), 1–18.
Eisele, J., W. Abouchami, S. J. Galer, and A. W. Hofmann (2003), The 320 kyr Pb isotope evolution of Mauna Kea lavas recorded in the HSDP-2 drill core, *Geochem. Geophys. Geosyst.*, *4*(5), 8710, doi:10.1029/2002GC000339.
Escrig, S., A. Bézos, S. L. Goldstein, C. H. Langmuir, and P. J. Michael (2009), Mantle source variations beneath the Eastern Lau Spreading Center and the nature of subduction components in the Lau basin–Tonga arc system, *Geochem. Geophys. Geosyst.*, *10*, Q04014, doi: 10.1029/2008GC002281.
Escrig, S., A. Bézos, C. H. Langmuir, P. J. Michael and R. Arculus (2012), Characterizing the effect of mantle source, subduction input and melting in the Fonualei Spreading Center, Lau Basin: Constraints on the origin of the boninitic signature of the back-arc lavas, *Geochem. Geophys. Geosyst.*, *13*, Q10008, doi:10.1029/2012GC004130.
Ewart, A., K. D. Collerson, M. Regelous, J. I. Wendt, Y. Niu (1998), Geochemical evolution within the Tonga–Kermadec–Lau arc–back-arc systems: The role of varying mantle wedge composition in space and time, *J. Petrol.*, *39*, 331–368.
Falloon, T. J., and A. J. Crawford (1991), The petrogenesis of high-calcium boninite lavas dredged from the northern Tonga ridge, *Earth Planet. Sci. Lett.*, *102*(3), 375–394.
Falloon, T. J., and L. V. Danyushevsky (2000), Melting of refractory mantle at 1· 5, 2 and 2·5 GPa under anhydrous and H2O-undersaturated conditions: Implications for the petrogenesis of high-Ca boninites and the influence of subduction components on mantle melting, *J. Petrol.*, *41*(2), 257–283.
Falloon, T. J., D. H. Green, and A. J. Crawford (1987), Dredged igneous rocks from the northern termination of the Tofua magmatic arc, Tonga and adjacent Lau Basin, *Aust. J. Earth Sci.*, *34*(4), 487–506.
Falloon, T. J., A. Malahoff, L. P. Zonenshaina, and Y. Bogdanova (1992), Petrology and geochemistry of back-arc basin basalts from Lau Basin spreading ridges at 15, 18 and 19 S, *Mineral. Petrol.*, *47*(1), 1–35.
Falloon, T. J., L. V. Danyushevsky, T. J. Crawford, R. Maas, J. D. Woodhead, S. M. Eggins, S. H. Bloomer, D. J. Wright, S. K. Zlobin, and A. R. Stacey (2007), Multiple mantle plume components involved in the petrogenesis of subduction-related lavas from the northern termination of the Tonga Arc and northern Lau Basin: Evidence from the geochemistry of arc and backarc submarine volcanics, *Geochem. Geophys. Geosyst.*, *8*, Q09003, doi:10.1029/2007GC001619.
Falloon, T. J., L. V. Danyushevsky, A. J. Crawford, S. Meffre, J. D. Woodhead, and S. H. Bloomer (2008), Boninites and adakites from the northern termination of the Tonga Trench: Implications for adakite petrogenesis, *J. Petrol.*, *49*(4), 697–715.
Farley. K. A., J. Natland, and H. Craig (1992), Binary mixing of enriched and undegassed (primitive?) mantle components (He, Sr, Nd, Pb) in Samoan lavas, *Earth Planet. Sci. Lett.*, *111*, 183–199.
Fretzdorff, S., U. Schwarz-Schampera, H. L. Gibson, C.-D. Garbe-Schönberg, F. Hauff, and P. Stoffers (2006), Hydrothermal activity and magma genesis along a propagating back-arc basin: Valu Fa Ridge (southern Lau Basin), *J. Geophys. Res.*, *111*, B08205, doi:10.1029/2005JB003967.
Gale, A., C. A. Dalton, C. H. Langmuir, Y. Su, and J. G. Schilling (2013), The mean composition of ocean ridge basalts, *Geochem. Geophys. Geosyst.*, *14*, 489–518, doi:10.1029/2012GC004334.
Gill, J. B. (1984), Sr-Pb-Nd isotopic evidence that both MORB and OIB sources contribute to ocean island arc magmas in Fiji, *Earth Planet. Sci. Lett.*, *68*, 443–458.
Haase, K. M., S. Fretzdorff, R. Mühe, D. Garbe-Schönberg, and P. Stoffers (2009), A geochemical study of off-axis seamount lavas at the Valu Fa Ridge: Constraints on magma genesis and slab contributions in the southern Tonga subduction zone, *Lithos*, *112*, 137–148, doi: 10.1016/j.lithos.2009.05.041.
Hahm, D., D. R. Hilton, P. R. Castillo, J. W. Hawkins, B. B. Hanan, and E. H. Hauri (2012), An overview of the volatile systematics of the Lau Basin â€"Resolving the effects of source variation, magmatic degassing and crustal contamination, *Geochim. Cosmochim. Acta*, *85*, 88–113, doi:10.1016/j.gca.2012.02.007.
Hanyu, T. (2014), Deep plume origin of the Louisville hotspot: Noble gas evidence, *Geochem. Geophys. Geosyst.*, *15*, 565–576, doi:10.1002/2013GC005085.
Hanyu, T., et al. (2011), Geochemical characteristics and origin of the HIMU reservoir: A possible mantle plume source in the lower mantle, *Geochem. Geophys. Geosyst.*, *12*, Q0AC09, doi:10.1029/2010GC003252.
Hart, S. R., W. E. Glassley, and D. E. Karig (1972), Basalts and sea-floor spreading behind the Mariana Island arc, *Earth Planet. Sci. Lett.*, *15*, 12–18.
Hart, S. (1984), A large-scale isotope anomaly in the Southern Hemisphere mantle, *Nature*, *309*, 753–757.
Hart, S., and J. Blusztajn (2006), Age and geochemistry of the mafic sills, ODP site 1276, Newfoundland margin, *Chem. Geol.*, *235*, 222–237, doi:10.1016/j.chemgeo.2006.07.001.

Hart, S. R., and M. G. Jackson (2014), Ta'u and Ofu/Olosega volcanoes: The "Twin Sisters" of Samoa, their P, T, X melting regime, and global implications, *Geochem. Geophys. Geosyst.*, *15*, 2301–2318, doi:10.1002/2013GC005221.
Hauri, E. H., and S. Hart (1993), Re-Os isotope systematics of HIMU and EMII oceanic island basalts from the south Pacific Ocean, *Earth Planet. Sci. Lett.*, *114*(2), 353–371.
Hawkins, J. W., and J. Natland (1975), Nephelinites and basanites of the samoan linear volcanic chain and their possible tectonic significance, *Earth Planet. Sci. Lett.*, *24*, 427–439.
Hemond, C., C. Devey, and C. Chauvel (1994), Source compositions and melting processes in the Society and Austral plumes (South Pacific Ocean): Element and isotope (Sr, Nd, Pb, Th) geochemistry, *Chem. Geol.*, *115*(1), 7–45.
Hergt, J., and J. D. Woodhead (2007), A critical evaluation of recent models for Lau–Tonga arc–backarc basin magmatic evolution, *Chem. Geol.*, *245*, 9–44, doi:10.1016/j.chemgeo.2007.07.022.
Hilton, D. R., K. Hammerschmidt, G. Loock, and H. Friedrichsen (1993), Helium and argon isotope systematics of the central Lau Basin and Valu Fa Ridge: Evidence of crust/mantle interactions in a back-arc basin, *Geochim. Cosmochim. Acta*, *57*, 2819–2841.
Honda, M., D. B. Patterson, I. McDougall, and T. J. Falloon (1993), Noble gases in submarine pillow basalt glasses from the Lau Basin: Detection of a solar component in backarc basin basalts, *Earth Planet. Sci. Lett.*, *120*, 135–148.
Jackson, M. G., and S. Hart (2006), Strontium isotopes in melt inclusions from Samoan basalts: Implications for heterogeneity in the Samoan plume, *Earth Planet. Sci. Lett.*, *245*, 260–277, doi:10.1016/j.epsl.2006.02.040.
Jackson, M. G., S. R. Hart, J. G. Konter, A. A. P. Koppers, H. Staudigel, M. D. Kurz, J. Blusztajn, and J. M. Sinton (2010) Samoan hot spot track on a "hot spot highway": Implications for mantle plumes and a deep Samoan mantle source, *Geochem. Geophys. Geosyst.*, *11*, Q12009, doi:10.1029/2010GC003232.
Jackson, M. G., S. R. Hart, A. A. P. Koppers, H. Staudigel, J. Konter, J. Blusztajn, M. Kurz, and J. A. Russell (2007a), The return of subducted continental crust in Samoan lavas, *Nature*, *448*, 684–687, doi:10.1038/nature06048.
Jackson, M. G., M. Kurz, S. Hart, and R. K. Workman (2007b), New Samoan lavas from Ofu Island reveal a hemispherically heterogeneous high $^{3}He/^{4}He$ mantle, *Earth Planet. Sci. Lett.*, *264*, 360–374, doi:10.1016/j.epsl.2007.09.023.
Jackson, M. G., M. D. Kurz, and S. R. Hart (2009), Helium and neon isotopes in phenocrysts from Samoan lavas: Evidence for heterogeneity in the terrestrial high 3 He/4 He mantle, *Earth Planet. Sci. Lett.*, *287*(3), 519–528.
Jackson, M. G., S. R. Hart, J. G. Konter, M. D. Kurz, J. Blusztajn, and K. A. Farley (2014), Helium and lead isotopes reveal the geochemical geometry of the Samoan plume, *Nature*, *514*, 355–358, doi:10.1038/nature13794.
Jenner, F. E., R. J. Arculus, J. A. Mavrogenes, N. J. Dyriw, O. Nebel, and E. H. Hauri (2012), Chalcophile element systematics in volcanic glasses from the northwestern Lau Basin, *Geochem., Geophys., Geosys.*, *13*(6).
Johnson, K. T. M., ad J. M. Sinton (1990), Petrology, Tectonic Setting, and the Formation of Back-arc Basin Basalts in the North Fiji Basin, *Geol. Jahrb. Reihe D Heft*, *92*, 517–545.
Kessel, R., M. W. Schmidt, P. Ulmer, and T. Pettke (2005), Trace element signature of subduction-zone fluids, melts and supercritical liquids at 120–180 km depth, *Nature*, *437*(7059), 724–727.
Knaack, M. C., B. S. Cornelius, and P. R. Hooper (1994), Trace element analysis of rocks and minerals by ICP-MS, open file report, p. 10, GeoAnalytical Lab., Wash. State Univ.
Kogiso, T., Y. Tatsumi, G. Shimoda, and H. Barsczus (1997), High u (HIMU) ocean island basalts in southern Polynesia: New evidence for whole mantle scale recycling of subducted oceanic crust, *J. Geophys. Res.*, *102*, 8085–8103.
Konter, J. G., B. B. Hanan, J. Blichert-Toft, A. A.P. Koppers, T. Plank, and H. Staudigel (2008), One hundred million years of mantle geochemical history suggest the retiring of mantle plumes is premature, *Earth Planet. Sci. Lett.*, *275*, 285–295, doi:10.1016/j.epsl.2008.08.023.
Konter, J. G., and M. G. Jackson (2012), Large volumes of rejuvenated volcanism in Samoa: Evidence supporting a tectonic influence on late-stage volcanism, *Geochem. Geophys. Geosyst.*, *13*, Q0AM04, doi:10.1029/2011GC003974.
Konter, J. G., H. Staudigel, J. Blichert-Toft, B. B. Hanan, M. Polvé, G. R. Davies, N. Shimizu, P. Schiffman, and P. Schiffman (2009), Geochemical stages at Jasper Seamount and the origin of intraplate volcanoes, *Geochem. Geophys. Geosyst.*, *10*, Q02001, doi:10.1029/2008GC002236.
Koppers, A. A., H. Staudigel, and J. R. Wijbrans (2000), Dating crystalline groundmass separates of altered Cretaceous seamount basalts by the 40Ar/39Ar incremental heating technique, *Chemical Geology*, *166*(1), 139–158.
Koppers, A. A. P (2002), ArArCALC—software for 40 Ar/39 Ar age calculations, *Comput. Geosci.*, *28*(5), 605–619.
Koppers, A. A. P., H. Staudigel, J. R. Wijbrans, and M. S. Pringle (1998), The Magellan seamount trail: Implications for Cretaceous hotspot volcanism and absolute Pacific plate motion, *Earth Planet. Sci. Lett.*, *163*(1), 53–68.
Koppers, A. A. P., H. Staudigel, M. S. Pringle, and J. R. Wijbrans (2003), Short-lived and discontinuous intraplate volcanism in the South Pacific: Hot spots or extensional volcanism?, *Geochem. Geophys. Geosyst.*, *4*, 1089, doi:10.1029/2003GC000533.
Koppers, A. A., H. Staudigel, J. Phipps Morgan, and R. A. Duncan (2007), Nonlinear 40Ar/39Ar age systematics along the Gilbert Ridge and Tokelau Seamount Trail and the timing of the Hawaii-Emperor Bend, *Geochem. Geophys. Geosyst.*, *8*, Q06L13, doi:10.1029/2006GC001489.
Koppers, A. A. P., J. A. Russell, M. G. Jackson, J. Konter, H. Staudigel, and S. R. Hart (2008), Samoa reinstated as a primary hotspot trail, *Geology*, *36*(6), 435–438.
Koppers, A. A. P., J. A. Russell, J. Roberts, M. G. Jackson, J. G. Konter, D. J. Wright, H. Staudigel, and S. R. Hart (2011), Age systematics of two young en echelon Samoan volcanic trails, *Geochem. Geophys. Geosyst.*, *12*, Q07025, doi:10.1029/2010GC003438.
Kuiper, K. F., A. Deino, F. J. Hilgen, W. Krijgsman, P. R. Renne, and J. R. Wijbrans (2008), Synchronizing rock clocks of Earth history, *Science 320*(5875), 500–504.
Kurz, M. D., J. Curtice, D. E. Lott, and A. Solow (2004), Rapid helium isotopic variability in Mauna Kea shield lavas from the Hawaiian Scientific Drilling Project, *Geochem., Geophys., Geosyst.*, *5*(4).
Langmuir, C. H., A. Bezos, S. Escrig, and S. W. Parman (2006), Chemical systematics and hydrous melting of the mantle in back-arc basins, Back-Arc Spreading Systems: Geological, Biological, Chemical, and Physical Interactions, *Geophys. Monogr.*, edited by D. M. Christie, et al., vol. 166, 87 pp., AGU, Washington, D. C.
Lassiter, J. C., J. Blichert-Toft, E. H. Hauri, and H. G. Barsczus (2003), Isotope and trace element variations in lavas from Raivavae and Rapa, Cook–Austral islands: constraints on the nature of HIMU- and EM-mantle and the origin of mid-plate volcanism in French Polynesia, *Chem. Geol.*, *202*, 115–138, doi:10.1016/j.chemgeo.2003.08.002.
Le Bas, M. J. (2000), IUGS reclassification of the high-Mg and picritic volcanic rocks, *J. Petrol.*, *41*(10), 1467–1470.
Le Bas, M. J., R. W. Le Maitre, A. Streckeisen, and B. Zanettin (1986), A chemical classification of volcanic rocks based on the total alkali-silica disagram, *J. Petrol.*, *27*, 745–750.
Le Fèvre, B., and C. Pin (2001), An extraction chromatography method for Hf separation prior to isotopic analysis using multiple collection ICP-mass spectrometry, *Anal. Chem.*, *73*(11), 2453–2460.

Li, M., A. K. McNamara, and E. J. Garnero (2014), Chemical complexity of hotspots caused by cycling oceanic crust through mantle reservoirs, *Nat. Geosci.*, *7*, 366–370, doi:10.1038/ngeo2120.
Loock, G. (1990) Isotopic compositions of volcanic glasses from the Lau Basin, *Mar. Min.*, *9*, 235–246.
Lupton, J. E., R. J. Arculus, R. R. Greene, L. J. Evans, and C. I. Goddard (2009), Helium isotope variations in seafloor basalts from the Northwest Lau Backarc Basin: Mapping the influence of the Samoan hotspot, *Geophys. Res. Lett.*, *36*, L17313, doi:10.1029/2009GL039468.
Lupton, J. E., R. J. Arculus, F. E. Jenner, and R. R. Greene (2012a), Helium Isotope Variations in the Northern Lau and North Fiji Basins, Abstract V23B-2820 presented at 2012 Fall Meeting, AGU, San Francisco, Calif.
Lupton, J. E., J. Arculus, J. Resing, G. J. Massoth, R. R. Greene, L. J. Evans, and N. Buck (2012b), Hydrothermal activity in the Northwest Lau Backarc Basin: Evidence from water column measurements, *Geochem. Geophys. Geosyst.*, *13*, Q0AF04, doi:10.1029/2011GC003891.
Lytle, M. L., K. A. Kelley, E. H. Hauri, J. B. Gill, D. Papia, and R. J. Arculus (2012), Tracing mantle sources and Samoan influence in the northwestern Lau back-arc basin, *Geochem. Geophys. Geosyst.*, *13*, Q10019, doi:10.1029/2012GC004233.
Macdonald, G. A., and T. Katsura (1964), Chemical composition of Hawaiian Lavas, *J. Petrol.*, *5*, 83–133.
Martinez, F., and B. Taylor (2002), Mantle wedge control on back-arc crustal accretion, *Nature*, *416*(6879), 417–420.
Matsuda, J., K. Notsu, J. Okano, K. Yaskawa, and L. Chungue (1984), Geochemical implications from Sr isotopes and K-Ar age determinations for the Cook-Austral Island Chain, *Tectonophysics*, *104*(1), 145–154.
Maury, R. C., G. Guille, H. Guillou, C. Chauvel, P. Rossi, C. Pallares, and C. Legendre (2013), Temporal evolution of a Polynesian hotspot: New evidence from Raivavae (Austral islands, South Pacific ocean), *Bull. Soc. Geol. France*, *184*, 557–567.
McCulloch, M. T., and J. A. Gamble (1991), Geochemical and geodynamical constraints on subduction zone magmatism, *Earth Planet. Sci. Lett.*, *102*(3), 358–374.
McDonough, W. F., and S.-S. Sun (1995), The composition of the Earth, *Chem. Geol.*, *120*, 223–253.
McNamara, A. K., E. J. Garnero, and S. Rost (2010), Tracking deep mantle reservoirs with ultra-low velocity zones, *Earth Planet. Sci. Lett.*, *299*, 1–9, doi:10.1016/j.epsl.2010.07.042.
McNutt, M. K., D. W. Caress, J. Reynolds, K. A. Jordahl, and R. A. Duncan (1997), Failure of plume theory to explain midplate volcanism in the southern Austral islands, *Nature*, *389*(6650), 479–482.
Min, K., R. Mundil, P. R. Renne, and K. R. Ludwig (2000), A test for systematic errors in 40 Ar/39 Ar geochronology through comparison with U/Pb analysis of a 1.1-Ga rhyolite, *Geochim. Cosmochim. Acta*, *64*(1), 73–98.
Mukhopadhyay, S. (2012) Early differentiation and volatile accretion recorded in deep-mantle neon and xenon, *Nature*, *486*, 101–104, doi:10.1038/nature11141.
Nakamura, Y., and M. Tatsumoto (1988), Pb, Nd, and Sr isotopic evidence for a multicomponent source for rocks of Cook-Austral Islands and heterogeneities of mantle plumes, *Geochim. Cosmochim. Acta*, *52*, 2909–2924.
Nebel, O., and R. J. Arculus (2015), Selective ingress of a Samoan plume component into the northern Lau backarc basin, *Nat. Commun.*, *6*.
Nishio, Y., S. Sasaki, T. Gamo, H. Hiyagon, and Y. Sano (1998), Carbon and helium isotope systematics of North Fiji Basin basalt glasses: Carbon geochemical cycle in the subduction zone, *Earth Planet. Sci. Lett.*, *154*, 127–138.
Nohara, M., K. Hirose, J.-P. Eissen, T. Urabe, and M. Joshima (1994), The North Fiji Basin basalts and their magma sources: Part II. Sr-Nd isotopic and trace element constraints, *Mar. Geol.*, *116*, 179–195.
Pearce, J. A., M. Ernewein, S. H. Bloomer, L. M. Parson, B. J. Murton, and L. E. Johnson (1994), Geochemistry of Lau Basin volcanic rocks: influence of ridge segmentation and arc proximity, Special Publications, *Geol. Soc.*, *81*(1), 53–75, London, U. K.
Pearce, J. A., and P. T. Robinson (2010), The Troodos ophiolitic complex probably formed in a subduction initiation, slab edge setting, *Gondwana Res.*, *18*(1), 60–81.
Pearce, J. A., and R. J. Stern (2006), Origin of back-arc basin magmas: Trace element and isotope perspectives, in *Chemical Systematics and Hydrous Melting of the Mantle in Back-Arc Basins*, edited by D. M. Christie et al., pp 63–86, AGU, Washington, D. C.
Pearce, J. A., P. D. Kempton, and J. B. Gill (2007), Hf-Nd evidence for the origin and distribution of mantle domains in the SW Pacific, *Earth Planet. Sci. Lett.*, *260*, 98–114.
Peate, D., J. A. Pearce, C. J. Hawkesworth, H. Colley, C. M. H. Edwards, and K. Hirose (1997), Geochemical variations in Vanuatu Arc Lavas: The role of subducted material and a variable mantle wedge composition, *J. Petrol.*, *38*, 1331–1358.
Peate, D., T. Kokfelt, C. Hawkesworth, P. W. van Calsteren, J. M. Hergt, and J. A. Pearce (2001), U-series isotope data on Lau Basin Glasses: The role of subduction-related fluids during melt generation in back-arc Basins, *J. Petrol.*, *42*, 1449–1470.
Plank, T., and C. H. Langmuir (1998), The chemical composition of subducting sediment and its consequences for the crust and mantle, *Chem. Geol.*, *145*(3), 325–394.
Poreda, R. J., and H. Craig (1992), He and Sr isotopes in the Lau Basin mantle: Depleted and primitive mantle components, *Earth Planet. Sci. Lett.*, *113*, 487–493.
Price, A. A., M. G. Jackson, J. Blichert-Toft, P. S. Hall, J. M. Sinton, M. D. Kurz, and J. Blusztajn (2014), Evidence for a broadly distributed Samoan-plume signature in the northern Lau and North Fiji Basins, *Geochem. Geophys. Geosyst.*, *15*, 986–1008, doi:10.1002/2013GC005061.
Regelous, M., K. D. Collerson, A. Ewart, and J. I. Wendt (1997), Trace element transport rates in subduction zones: Evidence from Th, Sr and Pb isotope data for Tonga-Kermadec arc lavas, *Earth Planet. Sci. Lett.*, *150*, 291–302.
Regelous, M., S. Turner, T. J. Falloon, J. Gamble, and T. Green (2008), Mantle dynamics and mantle melting beneath Niuafo'ou Island and the northern Lau back-arc basin, *Contrib. Mineral. Petrol.*, *156*, 103–118, doi:10.1007/s00410-007-0276-7.
Regelous, M., J. A. Gamble, and S. P. Turner (2010), Mechanism and timing of Pb transport from subducted oceanic crust and sediment to the mantle source of arc lavas, *Chem. Geol.*, *273*, 46–54, doi:10.1016/j.chemgeo.2010.02.011.
Resing, J. A., et al. (2011), Active submarine eruption of boninite in the northeastern Lau Basin, *Nat. Geosci.*, *4*(11), 799–806.
Salters, V. J. M., and W. M. White (1998), Hf isotope constraints on mantle evolution, *Chem. Geol.*, *145*(3), 447–460.
Salters, V. J. M., S. Mallick, S. R. Hart, C. E. Langmuir, and A. Stracke (2011), Domains of depleted mantle: New evidence from hafnium and neodymium isotopes, *Geochem. Geophys. Geosyst.*, *12*, Q08001, doi:10.1029/2011GC003617.
Schiano, P., K. Burton, B. Dupre, J.-L. Birck, G. Guille, C. J. Allègre (2001), Correlated Os-Pb-Nd-Sr isotopes in the Austral-Cook chain basalts: The nature of mantle components in plume sources, *Earth Planet. Sci. Lett.*, *186*(3), 527–537.
Sobolev, A. V., and L. V. Danyushevsky (1994), Petrology and geochemistry of boninites from the north termination of the Tonga Trench: Constraints on the generation conditions of primary high-Ca boninite magmas, *J. Petrol.*, *35*(5), 1183–1211.
Staudigel, H., K. H. Park, M. Pringle, J. L. Rubenstone, W. H. F. Smith, and A. Zindler (1991), The longevity of the South Pacific isotopic and thermal anomaly, *Earth Planet. Sci. Lett.*, *102*(1), 24–44.
Steiger, R., and E. Jäger (1977), Subcommission on geochronology: Convention on the use of decay constants in geo-and cosmochronology, *Earth Planet. Sci. Lett.*, *36*(3), 359–362.

Su, Y. (2003), Global MORB chemistry compilation at the segment scale, PhD thesis, Dep. of Earth and Environ. Sci., Columbia Univ.
Tanaka, T., et al. (2000), JNdi-1: A neodymium isotopic reference in consistency with LaJolla neodymium, *Chem. Geol.*, *168*, 279–281.
Taylor, J. R. (1997), *An Introduction to Error Analysis: The Study of Uncertainties in Physical Measurements*, 327 pp., Univ. Sci. Books, Mill Valley, Calif.
Thompson, G., I. Smith, and J. Malpas (2001), Origin of oceanic phonolites by crystal fractionation and the problem of the Daly gap: An example from Rarotonga, *Contrib. Mineral. Petrol.*, *142*, 336–346, doi:10.1007/s004100100294.
Tian, L., P. R. Castillo, J. W. Hawkins, D. R. Hilton, B. B. Hannan, and A. J. Pietruszka (2008), Major and trace element and Sr–Nd isotope signatures of lavas from the Central Lau Basin: Implications for the nature and influence of subduction components in the back-arc mantle, *J. Volcanol. Geotherm. Res.*, *178*, 657–670, doi:10.1016/j.jvolgeores.2008.06.039.
Tian, L., P. R. Castillo, D. R. Hilton, J. W. Hawkins, B. B. Hanan, and A. J. Pietruszka (2011), Major and trace element and Sr-Nd isotope signatures of the northern Lau Basin lavas: Implications for the composition and dynamics of the back-arc basin mantle, *J. Geophys. Res.*, *116*, B11201, doi:10.1029/2011JB008791.
Timm, C., D. Bassett, I. J. Graham, M. I. Leybourne, C. E. J. de Ronde, J. Woodhead, D. Layton-Matthews, and A. B. Watts (2013), Louisville seamount subduction and its implication on mantle flow beneath the central Tonga–Kermadec arc, *Nat. Commun.*, *4*, 1720, doi:10.1038/ncomms2702.
Torsvik, T. H., K. Burke, B. Steinberger, S. J. Webb, and L. D. Ashwal (2010), Diamonds sampled by plumes from the core–mantle boundary, *Nature*, *466*, 352–355, doi:10.1038/nature09216.
Turner, D. L., and R. Jarrard (1982), K-Ar dating of the Cook-Austral Island Chain: A test of the hot-spot hypothesis, *J. Volcanol. Geotherm. Res.*, *12*(3), 187–220.
Turner, S., and C. Hawkesworth (1997), Constraints on flux rates and mantle dynamics beneath island arcs from Tonga-Kermadec lava geochemistry, *Nature*, *389*, 568–573.
Turner, S., and C. Hawkesworth (1998), Using geochemistry to map mantle flow beneath the Lau Basin, *Geology*, *26*, 1019–1022.
Turner, S., C. Hawkesworth, N. Rogers, J. Bartlett, T. Worthington, J. Hergt, J. Pearce, I. Smith (1997), ^{238}U-^{230}Th disequilibria, magma petrogenesis, and flux rates beneath the depleted Tonga-Kermadec island arc, *Geochem. Cosmochim. Acta*, *61*, 4855–4884.
Turner, S., J. Caulfield, T. Rushmer, M. Turner, S. Cronin, I. Smith, and H. Handley (2012), Magma evolution in the primitive, intra-oceanic Tonga arc: Rapid petrogenesis of dacites at Fonulaei volcano, *J. Petrol.*, *53*, 1231–1253.
Vanderkluysen, L., J. J. Mahoney, A. A. Koppers, C. Beier, M. Regelous, J. S. Gee, and P. F. Lonsdale (2014), Louisville Seamount Chain: Petrogenetic processes and geochemical evolution of the mantle source, *Geochem. Geophys. Geosyst.*, *15*, 2380–2400, doi:10.1002/2014GC005288.
Vervoort, J. D., P. J. Patchett, J. Blichert-Toft, and F. Albarède (1999), Relationships between Lu–Hf and Sm–Nd isotopic systems in the global sedimentary system, *Earth Planet. Sci. Lett.*, *168*(1), 79–99.
Volpe, A. M., J. D. Macdougall, and J. W. Hawkins (1988), Lau Basin basalts (LBB): Trace element and Sr-Nd isotopic evidence for heterogeneity in backarc basin mantle, *Earth Planet. Sci. Lett.*, *90*, 174–186.
Wasserburg, G. J., S. B. Jacousen, D. J. DePaolo, M. T. McCulloch, and T. Wen (1981), Precise determination of SmNd ratios, Sm and Nd isotopic abundances in standard solutions, *Geochim. Cosmochim. Acta*, *45*(12), 2311–2323.
Wendt, J. I., M. Regelous, K. D. Collerson, and A. Ewart (1997), Evidence for a contribution from two mantle plumes to island-arc lavas from northern Tonga, *Geology*, *25*, 611–614.
Weis, D., et al. (2006), High-precision isotopic characterization of USGS reference materials by TIMS and MC-ICP-MS, *Geochem. Geophys. Geosyst.*, *7*, Q08006, doi:10.1029/2006GC001283.
Wessel, P., and L. W. Kroenke (2008), Pacific absolute plate motion since 145 Ma: An assessment of the fixed hot spot hypothesis, *J. Geophys. Res.*, *113*, B06101, doi:10.1029/2007JB005499.
White, W. M., and J. Patchett (1984), Hf-Nd-Sr isotopes and incompatible element abundances in island arcs'' implications for magma origins and crust-mantle evolution, *Earth Planet. Sci. Lett.*, *67*, 167–185.
Woodhead, J. D. (1996) Extreme HIMU in an oceanic setting: The geochemistry of Mangaia Island (Polynesia), and temporal evolution of the Cook-Austral hotspot, *J. Volcanol. Geotherm. Res.*, *72*(1), 1–19.
Workman, R. K., and S. R. Hart (2005), Major and trace element composition of the depleted MORB mantle (DMM), *Earth Planet. Sci. Lett.*, *231*, 53–72, doi:10.1029/2003GC000568.
Workman, R. K., S. R. Hart, M. Jackson, M. Regelous, K. A. Farley, J. Blusztajn, M. Kurz, H. Staudigel (2004), Recycled metasomatized lithosphere as the origin of the Enriched Mantle II (EM2) end-member: Evidence from the Samoan Volcanic Chain, *Geochem. Geophys. Geosyst.*, *5*, Q04008, doi:10.1029/2003GC000623.
Wright, E., and W. M. White (1987), The origin of Samoa: New evidence from Sr, Nd, Pb isotopes, *Earth Planet. Sci. Lett.*, *81*, 151–162.
York, D. (1968), Least squares fitting of a straight line with correlated errors, *Earth Planet. Sci. Lett.*, *5*, 320–324.
Zindler, A. and S. Hart (1986), Chemical geodynamics. *Annual review of earth and planetary sciences*, *14*, 493–571.
Zellmer, K. E., and B. Taylor (2001), A three-plate kinematic model for Lau Basin opening, *Geochem. Geophys. Geosyst.*, *2*, 1020.
Zlobin, S. K., G. M. Kolesov, and N. N. Kononkova (1991), Development of within-plate magmatism on the landward and offshore slopes of the Tonga Trench, *Ofioliti*, *16*(1), 17–35.